

Channel Estimation and Hybrid Beamforming for Reconfigurable Intelligent Surfaces Assisted THz Communications

Boyu Ning, *Student Member, IEEE*, Zhi Chen, *Senior Member, IEEE*,
Wenrong Chen, Yiming Du, and Jun Fang, *Senior Member, IEEE*,

Abstract—Terahertz (THz) communications are promising to be the next frontier for wireless network but suffer from severe attenuation and poor diffraction. To address these challenges, this paper integrates two state-of-the-art technology, i.e., massive multiple input multiple output (MIMO) and reconfigurable intelligent surfaces (RISs), into THz communication to establish effective and stable connection. Owing to the passivity of the RISs, channel estimation remains an open problem, besides, traditional fully-digital beamforming (FDB) can not be applied in massive MIMO due to its high hardware cost. In sight of this, this paper develops a cooperative channel estimation procedure for RIS-assisted MIMO system via beam training that exploits the advantages of massive MIMO and poor scattering nature of THz channel. The whole procedure is developed based on cost-efficient hybrid beamforming (HB) architectures. Moreover, this paper designs two different codebooks for efficiently realizing the proposed estimation procedure via 3-tree hierarchical search. The two codebooks are referred to as tree dictionary (TD) codebook and phase shifter deactivation (PSD) codebook, with different advantages catering for various scenarios. Using the estimation information, this paper develops two closed-form transmission designs, i.e., direct allocation (DA) design and zero-forcing allocation (ZFA) design, for maximizing the overall spectral efficiency.

Index Terms—Terahertz communications, reconfigurable intelligent surfaces, channel estimation, hybrid beamforming, hierarchical codebook, massive MIMO.

I. INTRODUCTION

Data rate demands in wireless communications have grown rapidly in the last few decades. Due to this dramatical speed, the available bandwidths in the sub-6 gigahertz (GHz) and millimeter-wave (mmWave) bands will be tight for meeting data rate demands of diverse bandwidth-hungry applications. Terahertz (THz) communication (with frequency bands 0.1 – 10 THz) emerges as a promising technology to support explosive growth of data traffic [1]. Although THz communication enjoys the benefits that orders-of-magnitude increase in the bandwidth, it has two inevitable shortcomings in wireless propagations, i.e., *severe attenuation* and *poor diffraction*. The former one is not only due to the free-spread loss caused by high frequencies, but also the molecular absorption in the atmospheric medium. The latter one is owing to the short wavelength and the limited wave spread [2], [3]. On account of the above factors, the signal coverage areas are very limited and are easily blocked by opaque obstacles in THz communications [4], [5].

This work was supported in part by the National Natural Science Foundation of China under Grant 61571089 and 61631004.

B. Ning, Z. Chen, W. Chen, Y. Du, and J. Fang are with National Key Laboratory of Science and Technology on Communications, University of Electronic Science and Technology of China (UESTC), Chengdu 611731, China (e-mails: boyuning@outlook.com; chen zhi@uestc.edu.cn; wenrongchen@std.uestc.edu.cn; duyiming01009@163.com; junfang@uestc.edu.cn).

To alleviate the short-range bottleneck and realize uninterrupted wireless connectivity, massive multiple-input multiple-output (MIMO) [6] and reconfigurable intelligent surfaces (RISs) [7] can be seamlessly and sustainably integrated into THz communications for overcoming high pathloss and the case with line-of-sight (LoS) blockage, respectively. Despite the effectiveness of using massive antennas to combat pathloss, the increased transmit dimensions also complicate the signal processing and scale up hardware costs, as each antenna requires a dedicated radio frequency (RF) chain and an analog-to-digital converter (ADC) [8]. In practice, hybrid beamforming (HB) that implements part of MIMO beamforming in the analog domain using a phase array is the most promising approach for reducing hardware cost in massive MIMO systems [9]. On the other hand, RIS is a recent emerging hardware technology that broadening the signal coverage with reduced energy consumption and low-cost implementation [10]. What makes the RIS attractive compared to fixed reflector is the possibility to induce a certain phase shift independently on the incident electromagnetic by controllable meta-material [11], so as to dynamically alter the reflecting coverage. Different from conventional relay schemes, RISs enhance the transmission without receiving or transmitting signals, however, by altering the propagation environments in a passive way [12]. Hence, if the RISs are mounted on suitable positions for transmission assist, the LoS blocking problem in THz communication can be effectively solved. In light of this, in this paper, we integrate the three state-of-the-art technologies, i.e., THz communication, massive MIMO, and RIS-assisted transmission, in wireless system for expected mutualistic symbiosis.

A. Prior Work

Comparing to traditional fully-digital beamforming (FDB) architecture, which precodes data stream $\mathbf{s} \in \mathbb{C}^{N_s}$ using N_t antennas and N_t RF chains with $\mathbf{x} = \mathbf{F}_{DS}\mathbf{s}$, HB architecture preprocesses the data streams in a non-linear way with only N_{RF} RF chains, $N_s \leq N_{RF} \ll N_t$, by combining the analog precoder \mathbf{F}_{RF} and the digital precoder \mathbf{F}_B as $\mathbf{x} = \mathbf{F}_{RF}\mathbf{F}_B\mathbf{s}$. Due to the classic digital MIMO techniques (e.g., right singular vectors and channel inversion) can not be directly applied under the analog hardware constraints, active researches have been conducted on finding new solutions satisfying HB architecture. A promising approach to the HB designs lies in the concept of reconstructing the optimal FDB solution, i.e., $\mathbf{F}_{RF}\mathbf{F}_B = \mathbf{F}_D^{\text{opt}}$. For single-data stream transmission, [13] states that an arbitrary complex vector can be realized as the addition of two phase shift vectors, that is, the optimal FDB solution can be reconstructed by HB architecture with only two RF chains. For multi-data streams transmission, [14] establishes that if $N_{RF} = 2N_s$, the HB structure can realize any FDB with closed-form exactly. From the reconstruction approach, we know that the HB does not

necessarily have inferior performance to FDB even with fewer RF chains in massive MIMO systems, i.e., $N_{RF} = 2N_s \ll N_t$. For further reducing the HB hardware complexity, it is of interest to study the cases with fewer number of RF chains ($N_s \leq N_{RF} < 2N_s$), especially when $N_s = N_{RF}$. In this case, two near-optimal closed-form solutions for analog precoder are shown in [15] and [16] that the analog precoder is set to the phase of the elements of the singular vectors of the channel matrix [15] in point-to-point scenario, and it is set to the phase of the channel matrix for K -user MISO systems [16]. A higher-performance numerical solution can be conducted by iterative coordinate descent (ICD) algorithm [14]. From another perspective, it is shown in [17] that the spectral efficiency maximization problem can be approximately solved by minimizing the Frobenius norm of the difference between the FDB and the HB, i.e., $\min \|\mathbf{F}_D^{\text{opt}} - \mathbf{F}_{RF}\mathbf{F}_B\|_F$. Based on this conclusion, an alternating minimization based on manifold optimization is proposed in [18], as well as a relaxed convex optimization based on matrix decomposition is provided in [19]. However, above solutions are all in the continuous domain, where infinite-resolution phase shifter is difficult to realize in practice. As a result, the researches on discrete phase shifters scheme [20] and array response analog precoder (ARAP)-based HB scheme [17] are of great significance for implementation. As for high frequency channel such as mmWave channel and THz channel, many advantages can be exploited by leveraging the beamspace channel representation introduced in [21]. This indicates that the designed analog precoders should be restricted to discrete fourier transform (DFT) vectors, which shifts the researches on beam training protocols [22]–[24], beam tracking procedures [25], [26] and beam-scanning codebooks designs [27]–[30].

RIS is a recent emerging technology that has been introduced into various wireless communication systems rapidly. In [31] and [32], an RIS-assisted single-input single-output (SISO) system is introduced with practical experiment results on maximizing achievable capacity and minimizing the link outage probability, respectively. Basar presented a general mathematical framework for the calculation of symbol error probability by deriving the distribution of the received signal-to-noise ratio (SNR) [33]. For RIS-assisted multiple-input single-output (MISO) systems, preliminary contributions focus on optimizing the RIS parameters for different objectives. The authors of [34]–[36] studied the optimization problems of maximizing the sum-rate and energy efficiency, while employing zero-forcing beamforming at the base station (BS). The authors of [37]–[39] consider joint active and passive beamforming optimization problems of maximizing the total received signal power. Both centralized and distributed algorithms were developed in [37], [38], and a more practical case that the RIS with only finite number of discrete phase shifts is extended in [39]. Such joint active and passive beamforming optimization problems are also investigated for maximizing the minimum SINR [40], the weighted sum-rate [41], the secrecy rate [42], and so on. It is worth noting that most of RIS optimizations for MISO systems can be directly transformed to quadratically constrained quadratic programs, while the design on RIS-aided MIMO systems with multiple antennas at both the transmitter and the receiver remains much more challenges and is still an open problem [43]–[45]. In addition, the aforementioned works [33]–[45] assumed the knowledge of the channel state information (CSI) on the new RIS-related channels are available. However, it is an intractable task since RIS can not transmit/receive signals due to the lack of active RF chains. Recently, several works

have focused on channel estimation for the RIS-assisted MISO systems [46]–[48]. Unfortunately, it is difficult to combine the existing estimation/beamforming solutions to cater for RIS-assisted THz massive MIMO systems with HB architecture. Even if it is feasible, the large-scale pilots and the optimization procedure by the existing approaches would result in high overhead.

B. Contributions and Organization

The problem of interest in this paper lies on realizing a low-complexity transmission strategy in RIS-assisted THz massive MIMO system. For practical implementation, we consider codebook-based RIS and ARAP-based HB at transceivers. Owing to the passivity of RISs (unable to transmit/receive signal), the *first challenge* remains since the traditional channel estimation approaches [49]–[51] are not applicable any more to RIS-assisted systems. On the other hand, the *second challenge* is attributed to the large-scale antenna arrays implemented in THz systems, which incurs high pilot overhead and costly time consumption [53]. In this paper, our first endeavour is to acquire the channel information of the RIS-assisted system. Using the obtained information, we aim to develop the designs of the hybrid precoder/combiners and the RISs, to maximize the overall spectral efficiency. The main contributions of the paper are summarized below.

- We consider an RIS-assisted THz MIMO system, where a multi-antenna BS serves K multi-antenna users with the assist of N_i RISs. For practical implementation, BS and users are using full-connected ARAP-based HB architecture with limited RF chains, and RISs are constrained by finite codewords. By exploiting the sparsity of THz channel and the characteristics of massive antenna array, a beam training manner is proposed as the basis for realizing channel measurement.
- We develop a cooperative estimation procedure to measure the overall RIS-assisted MIMO channels. Specifically, three phases are developed to achieve different groups of measurements. In phase 1, the deaf-mute RIS carries out a set of prescribed codewords sequentially, which are known to active transceivers. By leveraging the prescribed prior information, the best codeword for each RIS can be obtained by active terminals. In phase 2 and phase 3, the LoS links and the reflecting links are respectively measured by N predefined narrow beams on each side, via beam training. To reduce the search complexity, we adopt hierarchical tree search that incorporate the wide-beam search and the narrow-beam search by stages, rather than testing all $N \times N$ narrow-beam pairs one by one.
- We design two novel codebooks for efficient realization of the tree-search procedure. Specifically, each codebook is composed of the bottom-stage ARAP-based narrow beams codewords and the upper-stage wide beams codewords, respectively. While tree search schemes are widely adopted in bisection manner (2-tree) [26]–[29], [49]–[51], we show that 3-tree search is optimal among tree search schemes for most of cases (in terms of N). For narrow beams design, we stress the importance of designing these beams with common coverage-edge energy, based on which a direction distribution rule is developed. For wide beams design, we propose two approaches to complete the 3-tree codebooks, catering for various scenarios. The tree dictionary (TD) codebook has high anti-noise ability but each wide beam needs all RF chains. The phase shifter deactivation (PSD) codebook is sensitive to noise

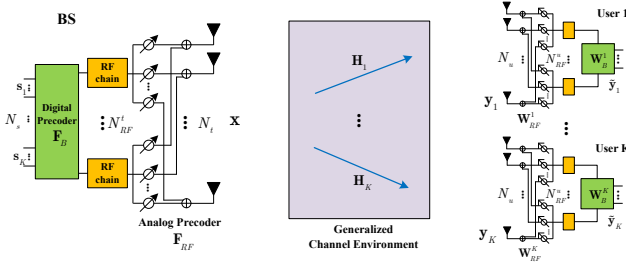


Fig. 1. A multi-user massive MIMO system with the HB architecture at the BS and the user terminals.

but each wide beam needs only one RF chain, thus the search time can be further reduced by simultaneously testing multi beams.

- We develop two closed-form transmission designs for maximizing the overall spectral efficiency. Specifically, we propose a direct allocation (DA) design for both signal-user case and multi-user case, and a zero-forcing allocation (ZFA) design dedicated to multi-user case. The advantage of the ZFA design appears at high-SNR regime. Moreover, in scheme using the DA design, all terminals need only partial channel information throughout the estimation procedure, which reduces estimation information transfer.

The remainder of the paper is organized as follows. Section II introduces the system model and problem statement for the channel estimation and the transmission design. The proposed framework of channel estimation procedure and design of RIS and hybrid precoder/combiner are presented in Section III and Section IV. Discussions and extensions are presented in Section V. Numerical results are provided in Section VI, and conclusions are drawn in Section VII.

Notation: Throughout the paper, we use small normal face for scalars, small bold face for vectors, capital bold face for matrices, \mathbb{C} for complex numbers, and \mathbb{N}^+ for positive integer respectively. $\mathbb{E}\{\cdot\}$, $\det(\cdot)$, $\text{tr}(\cdot)$, $|\cdot|$, $\|\cdot\|_p$ represents expectation, determinant, trace, modulus, and p -norm operator. The superscript $\{\cdot\}^T$, $\{\cdot\}^\dagger$, and $\{\cdot\}^H$ denote the transpose, conjugate, and Hermitian transpose respectively. $\mathbf{a}(n)$ and $\mathbf{A}(:, n)$ represents the n th element and n th column of its argument. $\text{card}[\cdot]$ denotes the cardinality of its set arguments and $\text{diag}(\cdot)$ denotes a diagonal matrix whose diagonal elements are given by its argument. $\lfloor \cdot \rfloor$ and $\lceil \cdot \rceil$ are the floor and ceiling function. $\text{mod}_n(\cdot)$ returns the remainder after division by n . \otimes and \odot are Kronecker product and Hadamard product operator. $\text{span}(\cdot)$ denotes the subspace spanned by the collection of vectors and \perp denotes the orthogonal complement of a subspace. \mathbf{I}_N denotes the $N \times N$ identity matrix.

II. SYSTEM MODEL AND PROBLEM STATEMENT

In this section, we present an RIS-assisted THz massive MIMO system as well as considered problems.

A. Massive MIMO with Hybrid Architectures

Consider a narrowband downlink multi-user massive MIMO system as depicted in Fig. 1, where BS with N_t antennas intends to send N_s data streams to serve K users, each with N_u antennas and D_k required data symbols. Since the implementation of fully-digital precoder/combiners with N_t/N_u RF chains suffers from high cost and power consumption, we consider a two-stage fully-connected hybrid digital and analog

architecture at all terminals, such that $N_s \leq N_{RF}^t \ll N_t$ and $D_k \leq N_{RF}^{u,k} \ll N_u$.

At the BS with hybrid precoder, a transmit vector $\mathbf{x} \in \mathbb{C}^{N_t}$ is generated via the following process. First, a data stream vector $\mathbf{s} \in \mathbb{C}^{N_s}$ which concatenates D_k required data symbols for user k , i.e., $N_s = \sum_{k=1}^K D_k$, is processed by a baseband digital precoder $\mathbf{F}_B \in \mathbb{C}^{N_{RF}^t \times N_s}$, and then up-converted to the RF domain by passing through N_{RF}^t RF chains before being precoded with an analog precoder $\mathbf{F}_{RF} \in \mathbb{C}^{N_t \times N_{RF}^t}$. The analog beamformer is implemented by a set of variable phase shifters and thus is subjected to magnitude constraint, i.e., $|\mathbf{F}_{RF}(i, j)| = 1$, $\forall i, j$. The normalized power constraint is given by $\|\mathbf{F}_{RF}\mathbf{F}_B\|_2^2 = 1$. Therefore, the transmitted signal by HB schemes can be written as

$$\mathbf{x} = \sqrt{P}\mathbf{F}_{RF}\mathbf{F}_B\mathbf{s} = \sqrt{P}\sum_{i=1}^K\mathbf{F}_{RF}\mathbf{F}_B^i\mathbf{s}_i, \quad (1)$$

where P is the total transmitted power. $\mathbf{F}_B^i \in \mathbb{C}^{N_{RF}^t \times D_i}$ and $\mathbf{s}_i \in \mathbb{C}^{D_i}$ are the subprecoders and the data stream vector for i th user, i.e., $\mathbf{F}_B = [\mathbf{F}_B^1, \mathbf{F}_B^2, \dots, \mathbf{F}_B^K]$ and $\mathbf{s} = [\mathbf{s}_1^T, \mathbf{s}_2^T, \dots, \mathbf{s}_K^T]^T$. Here, we assume that $\mathbb{E}[\mathbf{s}\mathbf{s}^H] = \mathbf{I}_{N_s}$. For k th user, the received signal can be expressed as

$$\mathbf{y}_k = \sqrt{P}\mathbf{H}_k \left(\underbrace{\mathbf{F}_{RF}\mathbf{F}_B^k\mathbf{s}_k}_{\text{desired signal}} + \underbrace{\sum_{i \neq k}^K \mathbf{F}_{RF}\mathbf{F}_B^i\mathbf{s}_i}_{\text{interference signal}} \right) + \mathbf{n}, \quad (2)$$

where $\mathbf{H}_k \in \mathbb{C}^{N_u \times N_t}$ represents the matrix of complex channel gains from the N_t antennas of the BS to the antennas of the k th user. $\mathbf{n} \in \mathbb{C}^{N_u}$ is zero-mean additive white Gaussian noise. Without loss of generality, we assume unit variance of the noise terms for all user, i.e., $\mathbf{n} \sim \mathcal{CN}(\mathbf{0}, \sigma_n^2 \mathbf{I}_{N_u})$. At user k , the received signal $\mathbf{y}_k \in \mathbb{C}^{N_u}$ is first processed by an analog combiner $\mathbf{W}_{RF}^k \in \mathbb{C}^{N_u \times N_{RF}^{u,k}}$, implemented by phase shifters such that $|\mathbf{W}_{RF}^k(i, j)| = 1$, $\forall i, j$, then down-converted to the digital domain via $N_{RF}^{u,k}$ RF chains and processed by a baseband digital combiner $\mathbf{W}_B^k \in \mathbb{C}^{N_{RF}^{u,k} \times N_u}$, which results in the final signal as

$$\tilde{\mathbf{y}}_k = \sqrt{P}\mathbf{W}_k^H\mathbf{H}_k\mathbf{x}_{ds} + \underbrace{\sqrt{P}\mathbf{W}_k^H\mathbf{H}_k\mathbf{x}_{is} + \mathbf{W}_k^H\mathbf{n}}_{\text{effective noise}}, \quad (3)$$

where $\mathbf{x}_{ds} = \mathbf{F}_{RF}\mathbf{F}_B^i\mathbf{s}_i$, $\mathbf{x}_{is} = \sum_{i \neq k}^K \mathbf{F}_{RF}\mathbf{F}_B^i\mathbf{s}_i$, and $\mathbf{W}_k = \mathbf{W}_{RF}^k\mathbf{W}_B^k$. We mention that the uplink expression of considered system for k th user is identical to (3) with the roles of the precoders and combiners switched under transposed reciprocal channel, i.e., $\mathbf{H} \rightarrow \mathbf{H}^T$.

B. RIS-assisted THz Channel Model

The high pathloss significantly limits scattering in THz communication, where the power of scattering components is much lower (more than 20dB) than that of LoS component [4]. Thus, THz channel is sparse with line-of-sight (LoS) dominant and sensitive to LoS-blocking obstacles [5]. To overcome this, this paper consider such channel environment that N_i RISs are installed on surrounding wall to enhance the signal coverage and communication quality by providing tunable strong reflecting component, as shown in Fig. 2. Since the scattering components and/or weak NLoS components (reflected by other

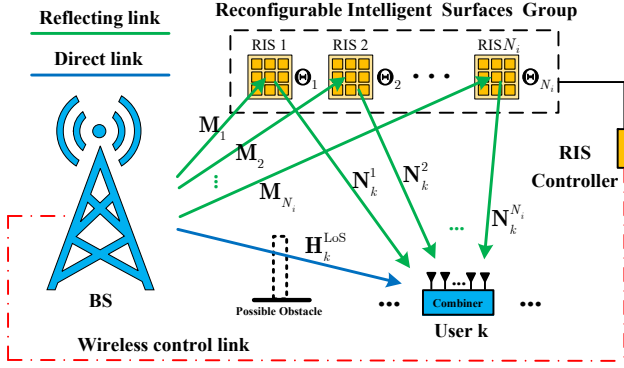


Fig. 2. Channel environment for k th user, i.e., channel \mathbf{H}_k .

surfaces) are negligible, the k th user channel can be modelled as

$$\mathbf{H}_k(f, \mathbf{d}_k) = G_t G_r \left[\mathbf{H}_k^{\text{LoS}}(f, d_{k,0}) + \sum_{l=1}^{N_i} \mathbf{H}_{k,l}^{\text{Ref}}(f, d_l^M, d_{k,l}^N) \right], \quad (4)$$

in which G_t and G_r are the transmit and receive antenna gains. $\mathbf{H}_k^{\text{LoS}}$ is the LoS channel between BS and k th user. In BS-RISs-user k link, $\{\mathbf{H}_{k,l}^{\text{Ref}}(f, d_l^M, d_{k,l}^N)\}_{l=1}^{N_i}$ are the strong reflecting channels provided by RISs. f is the carrier frequency and $\mathbf{d}_k = [d_{k,0}, d_1^M, d_{k,1}^N, \dots, d_{N_i}^M, d_{k,N_i}^N]$ is the vector of transmit distance in corresponding propagation paths. d_l^M (resp. $d_{k,l}^N$) is the distance between BS and l th RIS (resp. l th RIS and k th user). Each RIS can dynamically adjust N_r intelligent elements of the meta-surface to achieve phase shifts on the reflecting signal in a passive way (no energy amplification). Therefore, the received signal vector at the l th RIS can be linearly transformed by a diagonal phase-shift matrix $\Theta_l = \text{diag}(\beta e^{j\theta_l^1}, \beta e^{j\theta_l^2}, \dots, \beta e^{j\theta_{N_r}^l})$, $l = 1, \dots, N_i$, and reflected to k th user, where $j = \sqrt{-1}$, $\{\theta_i^j\}_{i=1}^{N_r} \in [0, 2\pi)$, and $\beta \in [0, 1]$ are imaginary unit, PSs, and amplitude reflection coefficient on the combined incident signal, respectively. Thus, as shown in Fig. 2, the N_i reflecting links to the user k provided by RISs in (4) can be expressed as

$$\sum_{l=1}^{N_i} \mathbf{H}_{k,l}^{\text{Ref}}(f, d_l^M, d_{k,l}^N) = \sum_{l=1}^{N_i} \eta \mathbf{N}_k^l(f, d_{k,l}^N) \Theta_l \mathbf{M}_l(f, d_l^M), \quad (5)$$

where η is the path-loss compensation factor (see 9). \mathbf{M}_l is the LoS channel between BS and the l th RIS, and \mathbf{N}_k^l is the LoS channel between the l th RIS and the user k . The area of each RIS is limited and only provides one strong reflecting path which is a cascade of a BS-RIS LoS channel and an RIS-user k LoS channel. Thus, the separate components of the k th user channel in (4) and (5) can be explicitly written as

$$\begin{aligned} \mathbf{H}_k^{\text{LoS}}(f, d_{k,0}) &= a(f, d_{k,0}) \mathbf{a}_{N_u}^U(\varphi_{U,H}^k) \mathbf{a}_{N_t}^B(\varphi_{B,H}^k)^H, \\ \mathbf{M}_l(f, d_l^M) &= a(f, d_l^M) \mathbf{a}_{N_r}^R(\varphi_{R,M}^l) \mathbf{a}_{N_t}^B(\varphi_{B,M}^l)^H, \\ \mathbf{N}_k^l(f, d_{k,l}^N) &= a(f, d_{k,l}^N) \mathbf{a}_{N_u}^U(\varphi_{U,N}^{l,k}) \mathbf{a}_{N_r}^B(\varphi_{R,N}^{l,k})^H, \end{aligned} \quad (6)$$

where $k = 1, \dots, K$, $l = 1, \dots, N_i$ and $a(f, d)$ is the path loss. Considering the rank-one channel \mathbf{M}_l in (6), each RIS can only serve one data stream as well as one user. Let $\mathbb{L}(k)$ denotes the RIS allocation set for user k , we have $\text{card}[\mathbb{L}(k)] = D_k - 1$. In THz communication, the molecular absorption loss

drastically affects the channel. Thus, $a(f, d)$ consists of the free-spread loss and the molecular absorption loss as [3]

$$a(f, d) = \frac{c}{4\pi f d} e^{-\frac{1}{2}\tau(f)d}, \quad (7)$$

where c stands for the speed of light and $\tau(f)$ is the medium absorption factor. According to the path loss of the far-field RIS-assisted beamforming case [52], the cascade path loss of BS-RIS l -user k link is supposed to satisfy

$$G_t G_r \eta a(f, d_l^M) a(f, d_{k,l}^N) = \frac{G_t G_r G_{N_r} c}{8\sqrt{\pi^3} f d_l^M d_{k,l}^N} e^{-\frac{1}{2}\tau(f)(d_l^M + d_{k,l}^N)}. \quad (8)$$

where G is the RIS element gain. Thus, the path-loss compensation factor is given as

$$\eta = \frac{2\sqrt{\pi} f G_{N_r}}{c}. \quad (9)$$

In (6), the variable φ is the path's azimuth AoD/AoA¹. Further, $\mathbf{a}_{N_a}^E(\phi)$ is the normalized antenna array response vectors at terminal E with N_a antenna elements. For simplicity of exposition, (6) considers a ULA configuration such as

$$\mathbf{a}_{N_a}(\phi) = \frac{1}{\sqrt{N_a}} [1, e^{jk d_a \sin(\phi)}, \dots, e^{jk d_a (N-1) \sin(\phi)}]^T, \quad (10)$$

where $k = 2\pi/\lambda$, λ is the wavelength and d_a is the antenna spacing.

C. Problem Statement

In this paper, we assume that the BS, the RISs and the users are all movable and all terminals have no prior knowledge of any channel. Hence, our first endeavour is to acquire the channel information. Given the geometric THz channel model in (6), estimating the channel is equivalent to estimating the multipath components, i.e., the AoAs, the AoDs and the gain of each path. As shown in Fig. 3, the primary structure of the overall channels estimation is substantially a triangular three-node structure, of which the main parameters include six angles $\varphi_{B,M}^l, \varphi_{B,H}^k, \varphi_{R,M}^l, \varphi_{R,N}^{l,k}, \varphi_{U,H}^k, \varphi_{U,N}^{l,k}$. For BS-user link, a feasible transmission strategy is to steer analog beam pointing at corresponding AoD/AoA ($\varphi_{B,H}^k$ and $\varphi_{U,H}^k$) at the transceivers [22]–[28], [30]. For BS-RIS-user link, we show that the strategy can be considered in the same way since structure of the effective reflecting channel is the same as $\mathbf{H}_k^{\text{LoS}}$, i.e.,

$$\begin{aligned} & \frac{\mathbf{N}_k^l \Theta_l \mathbf{M}_l}{a(f, d_{k,l}^N) a(f, d_l^M)} \\ &= \mathbf{a}_{N_u}^U(\varphi_{U,N}^{l,k}) \underbrace{\mathbf{a}_{N_r}^B(\varphi_{R,N}^{l,k})^H \Theta_l \mathbf{a}_{N_r}^R(\varphi_{R,M}^l) \mathbf{a}_{N_t}^B(\varphi_{B,M}^l)^H}_{\text{effective gain (scalar)}}, \end{aligned} \quad (11)$$

where the design of RIS is equivalent to maximize the effective gain, and one optimal solution is (proof see Appendix A)

$$\begin{aligned} \Theta_l^{\text{opt}} &= \text{diag}(\beta e^{j\theta_l^1}, \beta e^{j\theta_l^2}, \dots, \beta e^{j\theta_{N_r}^l}), \\ \theta_n &= k d_a (n-1) \underbrace{(\sin \varphi_{R,N}^{l,k} - \sin \varphi_{R,M}^l)}_{\Delta_{l,k}}, \quad n = 1, \dots, N_r. \end{aligned} \quad (12)$$

¹For explicit φ , the subscript U, R, and B represent the user, RIS, and BS; and the subscript H, M, and N represent the channel \mathbf{H} , \mathbf{M} , and \mathbf{N} respectively. The superscript l and k represents the l th RIS and k th user.

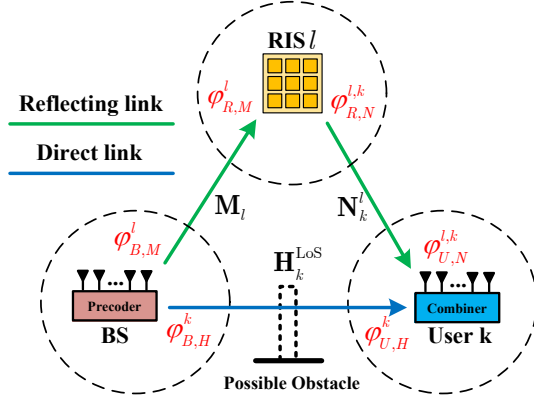


Fig. 3. Primary three-node structure of RIS-assisted massive MIMO systems.

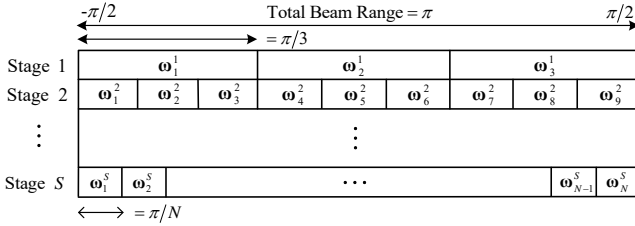


Fig. 4. Beam coverage structure of 3-tree hierarchical codebook.

In such case, the design for the transceivers needs only local angles (inside the dotted circle in Fig. 3) and the design for RIS need only $\Delta_{l,k}$ (we do not need explicit $\phi_{R,N}^{l,k}$ and $\phi_{R,M}^l$). As a result, only partial CSI (four angles, $\Delta_{l,k}$ and path loss) is required in estimation procedure. Inspired by these ideas, we will develop a cooperative estimation procedure along with hierarchical codebook for the beam-training vectors to capture the partial CSI, using finite RIS codewords and the practical ARAP-based HB [17] such as

$$|\mathbf{F}_{RF}(:, i)| \in \mathcal{F}_{RF} = \{\mathbf{a}_{N_a}(\varphi_1), \dots, \mathbf{a}_{N_a}(\varphi_N)\}, \forall i. \quad (13)$$

Using the obtained partial CSI, we will derive the RIS and HB solutions to maximize the overall spectral efficiency.

III. CHANNEL ESTIMATION PROCEDURE

In this section, we focus on the AoA/AoD angles measurement by beam-training way. To this end, we need to find a narrow-beam pair with strongest power among total $N \times N$ narrow-beam pairs for each link, where N predefined narrow beams cover all directions on each side. To reduce the search time, we adopt a 3-tree hierarchical search that realizes the beam search stage by stage with wide beams and narrow beams, rather than exhaustively testing all narrow-beam pairs. Let ω_n^s denotes the n th beam vector in the s th stage, Fig. 4 shows the beam coverage structure of the 3-tree codebook and $S = \log_3^N$ is the bottom-stage number. We mention that it is important to design the bottom-stage ARAP-based narrow beams (design the number N and direction distribution), based on which the design of wide beams can be completed.

In the rest of this section, we first present the results of cooperative estimation procedure in Section III-A. Then, the narrow beams design and the wide beams design are further discussed in Section III-B and Section III-C, in which we will explain why we choose 3-tree search in proposed procedure.

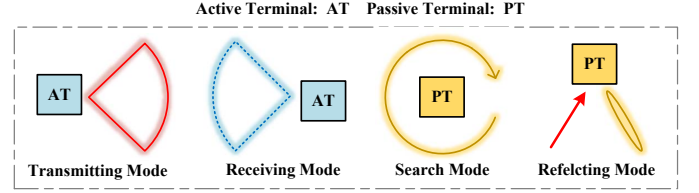


Fig. 5. Beam modes for active and passive terminals in our system.

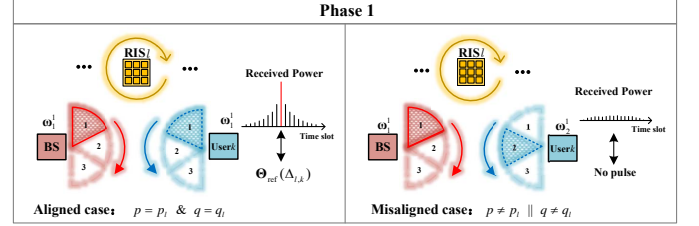


Fig. 6. Phase 1 of the cooperative channel estimation procedure.

A. Cooperative Channel Estimation Procedure

The active terminals (BS and user k) are capable of transmitting/receiving beams, while the passive terminal (RIS) is only able to reflect beams. As shown in Fig. 5, we define four general modes for the exposition in the rest of this paper.

- **Transmitting Mode:**

We use solid red line to represent the transmitting beams. In the transmitting mode, the terminal use ω as the precoder to form beam in certain range. In ideal case, if the AoD of a propagation link \mathbf{H} is within the beam range, we have $\|\mathbf{H}\omega\|_2 \gg 0$, otherwise, we have $\|\mathbf{H}\omega\|_2 \rightarrow 0$.

- **Receiving Mode:**

The solid-broken blue line denotes the receiving beams. In the receiving mode, the terminal use ω as the combiner to detect the signal in certain range, so as to further determine whether there exists path. In ideal case, if the AoA of a propagation link \mathbf{H} is in the beam range, we have $\|\omega^H \mathbf{H}\|_2 \gg 0$, otherwise, $\|\omega^H \mathbf{H}\|_2 \rightarrow 0$.

- **Reflecting Mode:**

The reflecting mode is to set RIS in such a form

$$\Theta_{\text{ref}}(x) = \text{diag}(\beta e^{j\theta_1}, \beta e^{j\theta_2}, \dots, \beta e^{j\theta_{N_r}}), \quad (14)$$

$$\theta_n = kd_a(n-1)x, \quad n = 1, \dots, N_r.$$

It is easy to verify that when any narrow-beam vector \mathbf{a}_{N_r} goes through $\Theta_{\text{ref}}(x)$, the reflecting signal $\Theta_{\text{ref}}(x)\mathbf{a}_{N_r}$ still follows the narrow-beam structure as (10).

- **Search Mode:**

The search mode is for RIS to search $\Delta_{l,k}$ in (12). Since $\Delta_{l,k}$ lies in domain $[-2, 2]$, we uniformly sample N points on it for codewords. In this mode, RIS tests $\Theta_{\text{ref}}(-2 + \frac{4i-2}{N})$, $i = 1, \dots, N$, one by one in predefined time slots, which are known in system.

To obtain the required CSI, three phases are developed to achieve different groups of measurements in a cooperative way, stated as following.

1) **Phase 1 (see Fig. 6):** In Phase 1, we aim to obtain $\Delta_{l,k}$, the necessary condition for which is that the BS can transmit enough power to RIS and the user k can receive enough reflecting power from RIS. Since the omni-transmitting/omni-receiving is impracticable in high-pathloss THz communication systems, we test 9 wide-beam pairs for satisfying this necessary condition. The 9 beam pairs are tested in 9 successive intervals with BS using $\{\omega_p^1\}_{p=1,2,3}$ in transmitting

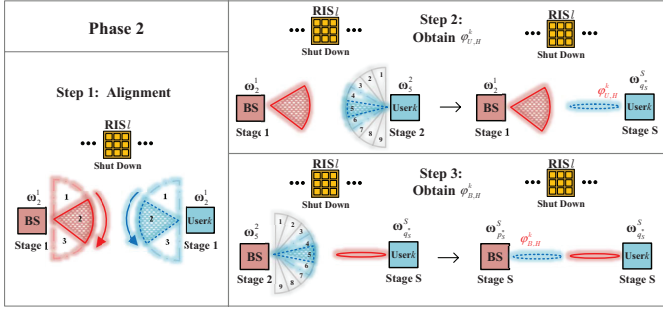


Fig. 7. Phase 2 of the cooperative channel estimation procedure.

mode and user k employing $\{\omega_q^1\}_{q=1,2,3}$ in receiving mode. The resulting signal in one interval can be expressed as

$$y_{q,p} = \sqrt{P}(\omega_q^1)^H \mathbf{H}_k \omega_p^1 s + n, \quad (15)$$

where $s = 1$ is the normalized pilot signal. In each interval, all RIS l ($l \in \mathbb{L}(k)$) carry search mode simultaneously on N time slots. For each RIS l , there is only one beam pair ($p_l \times q_l$) that covers both the BS-RIS l link and RIS l -user k link, i.e.,

$$(\omega_{q_l}^1)^H \mathbf{H}_{k,l}^{\text{Ref}} \omega_{p_l}^1 = \underbrace{(\omega_{q_l}^1)^H \mathbf{N}_k^l}_{\|(\omega_{q_l}^1)^H \mathbf{N}_k^l\|_2 \gg 0} \underbrace{\Theta_l \mathbf{M}_l \omega_{p_l}^1}_{\|\mathbf{M}_l \omega_{p_l}^1\|_2 \gg 0}. \quad (16)$$

During the interval of using this beam pair (aligned case), user k will detect an energy pulse on time slot when RIS l is carrying on $\Theta_l = \Theta_{\text{ref}}(\Delta_{l,k})$, i.e.,

$$\begin{aligned} \Delta_{l,k} &= \arg \max_x (\omega_{q_l}^1)^H \mathbf{N}_k^l \Theta_{\text{ref}}(x) \mathbf{M}_l \omega_{p_l}^1 \\ \text{s.t. } x &= -2 + \frac{4i-2}{N}, \quad i = 1, \dots, N. \end{aligned} \quad (17)$$

We note that each RIS is able to use spatial modulation to label identity information [33]. Thus, user k can utilize the pulse slots plus identity information to estimate $\Delta_{l,k}$.

2) *Phase 2 (see Fig. 7)*: In Phase 2, we aim to obtain $\varphi_{B,H}^k$ and $\varphi_{U,H}^k$ by three steps. Shutting down all RIS l , BS and user k search the narrow-beam pair of the link $\mathbf{H}_k^{\text{LoS}}$ cooperatively by 3-tree hierarchical search stage by stage. In step 1, 9 wide-beam pairs are tested by (15) for alignment and the resulting signals in stage 1 can be written in a vector as

$$\begin{aligned} \mathbf{y}_1^{\text{Ues}} &= \sqrt{P} \text{vec}(G_t G_r \mathbf{Q}_1^H \mathbf{H}_k^{\text{LoS}} \mathbf{P}_1 + \mathbf{N}_{\text{noise}}) \\ &= \sqrt{P} G_t G_r (\mathbf{P}_1^T \otimes \mathbf{Q}_1^H) \text{vec}(\mathbf{H}_k^{\text{LoS}}) + \mathbf{n} \\ &= c_k (\mathbf{P}_1^T \otimes \mathbf{Q}_1^H) \left[\mathbf{a}_{N_t}^B (\varphi_{B,H}^k)^{\dagger} \otimes \mathbf{a}_{N_u}^U (\varphi_{U,H}^k) \right] + \mathbf{n} \\ &= c_k \left[\mathbf{P}_1^T \mathbf{a}_{N_t}^B (\varphi_{B,H}^k)^{\dagger} \right] \otimes \left[\mathbf{Q}_1^H \mathbf{a}_{N_u}^U (\varphi_{U,H}^k) \right] + \mathbf{n}. \end{aligned} \quad (18)$$

where $\mathbf{P}_1 = \mathbf{Q}_1 = [\omega_1^1, \omega_2^1, \omega_3^1]$, $\mathbf{N}_{\text{noise}}$ is the noise matrix and $c_k = \sqrt{P} G_t G_r a(f, d_{k,0})$. User k compares the received power in 9 intervals and determines the aligned pair with the maximum received power, i.e., $n^* = \arg \max_n [\mathbf{y}_1^{\text{Ues}} \odot (\mathbf{y}_1^{\text{Ues}})^{\dagger}](n)$. The aligned pair is labeled by recording the beam choice of both sides with $p_1^* = \lfloor n^*/3 \rfloor$ and $q_1^* = \text{mod}_3(n^*)$, which completes the alignment of the first step. In step 2, BS transmits wide beam $\omega_{p_1^*}^1$ and user k uses hierarchical search by codewords in stage $s = 2, \dots, S$ to obtain $\varphi_{U,H}^k$. Thus, the resulting signals in stage s can be written as

$$\mathbf{y}_s^{\text{Ues}} = \sqrt{P} G_t G_r \mathbf{Q}_s^H \mathbf{H}_k^{\text{LoS}} \omega_{p_1^*}^1 + \mathbf{n}, \quad (19)$$

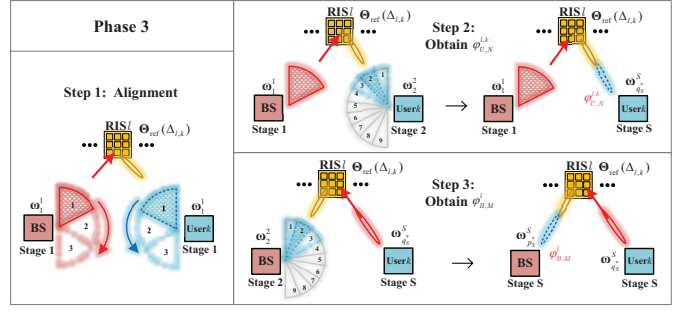


Fig. 8. Phase 3 of the cooperative channel estimation procedure.

where $\mathbf{Q}_s = [\omega_{3q_{s-1}^*-2}^s, \omega_{3q_{s-1}^*-1}^s, \omega_{3q_{s-1}^*}^s]$. Meanwhile, we calculate the parameters $q_s^* = 3q_{s-1}^* + \arg \max_n [\mathbf{y}_s^{\text{Ues}} \odot (\mathbf{y}_s^{\text{Ues}})^{\dagger}](n)$ to choose \mathbf{Q}_{s+1} for next stage. By recursively repeating above procedure, user k can find the desired narrow beam in stage S and the angle $\varphi_{U,H}^k$ is estimated by the direction of $\omega_{q_s^*}^s$. In step 3, user k transmit narrow beam $\omega_{q_s^*}^s$ and BS uses hierarchical search in the same way to obtain $\varphi_{B,H}^k$ and the resulting signals in stage $s = 2, \dots, S$ can be written as

$$\mathbf{y}_s^{\text{Bes}} = \sqrt{P} G_t G_r \mathbf{P}_s^H (\mathbf{H}_k^{\text{LoS}})^T \omega_{q_s^*}^s + \mathbf{n}, \quad (20)$$

where $\mathbf{P}_s = [\omega_{3p_{s-1}^*-2}^s, \omega_{3p_{s-1}^*-1}^s, \omega_{3p_{s-1}^*}^s]$ and we calculate the parameters $p_s^* = 3p_{s-1}^* + \arg \max_n [\mathbf{y}_s^{\text{Bes}} \odot (\mathbf{y}_s^{\text{Bes}})^{\dagger}](n)$ to choose \mathbf{P}_{s+1} for next stage. Likewise, the angle $\varphi_{U,H}^k$ is estimated by the direction of $\omega_{p_s^*}^s$, and the pathloss $a(f, d_{k,0})$ is estimated by $|\mathbf{y}_s^{\text{Bes}}(n_s^*)|/\sqrt{P} G_t G_r$ in step 3.

3) *Phase 3 (see Fig. 8)*: In Phase 3, we aim to obtain $\varphi_{B,M}^l$ and $\varphi_{U,N}^{l,k}$ through three steps similar to Phase 2. With the obtained information in Phase 1, we fix all RIS l ($l \in \mathbb{L}(k)$) in reflecting mode with $\Theta_l = \Theta_{\text{ref}}(\Delta_{l,k})$. In this case, we have $D_k - 1$ RISs to optimally bridge the BS-RIS link and the RIS-user k link. Thus, there exists D_k propagation path from BS to user k , including BS-user k LoS path. Noting that the BS-user k link has been estimated in Phase 2, we assign the resulting codewords ($\omega_{p_s^*}^s$ and $\omega_{q_s^*}^s$) of this 1st estimated path to vectors \mathbf{m}_p^1 and \mathbf{m}_q^1 . To estimate the AoA and AoD of the rest $D_k - 1$ reflecting paths, we need to use $D_k - 1$ loops of the 3-tree search with small modification. Specifically, in each stage, the receiver needs to cancel out the contributions of the previously estimated links when determining the best beam. By this method, during the estimation of the L th path ($L = 2, \dots, D_k$), the effective received signals in step 1 are calculated as

$$\begin{aligned} \mathbf{y}_1^{\text{Ues}} &= \underbrace{\sqrt{P} \text{vec}(\mathbf{Q}_1^H \mathbf{H}_k \mathbf{P}_1 + \mathbf{N}_{\text{noise}})}_{\text{received power}} \\ &\quad - \underbrace{\sum_{n=1}^{L-1} \sqrt{P} \text{vec}(G_t G_r a_{\text{path}}^n \mathbf{Q}_s^H \mathbf{m}_q^n (\mathbf{m}_p^n)^H \mathbf{P}_1)}_{\text{calculated previous contribution}}. \end{aligned} \quad (21)$$

where \mathbf{m}_p^n , \mathbf{m}_q^n , and a_{path}^n are the resulting codewords and the pathloss of the n th previous-estimated path, respectively.

In step 2, the effective received signals are calculated as

$$\mathbf{y}_s^{\text{Ues}} = \sqrt{P} \mathbf{Q}_s^H \mathbf{H}_k \omega_{p_1^*}^1 + \mathbf{n} - \sum_{n=1}^{L-1} \sqrt{P} G_t G_r a_{\text{path}}^n \mathbf{Q}_s^H \mathbf{m}_q^n (\mathbf{m}_p^n)^H \omega_{p_1^*}^1. \quad (22)$$

In step 3, the effective received signals are calculated as

$$\mathbf{y}_s^{\text{Bes}} = \sqrt{P} \mathbf{P}_s^H \mathbf{H}_k^T \omega_{q_s^*}^S + \mathbf{n} - \sum_{n=1}^{L-1} \sqrt{P} G_t G_r a_{\text{path}}^n \mathbf{P}_s^H (\mathbf{m}_p^n)^\dagger (\mathbf{m}_q^n)^T \omega_{q_s^*}^S. \quad (23)$$

After $D_k - 1$ loops, we find $D_k - 1$ narrow-beam pairs of the reflecting links, and the angle $\varphi_{B,M}^l$, $\varphi_{U,N}^{l,k}$ and pathloss a_{path}^n are estimated by the corresponding narrow-beam pair.

The core algorithm of the whole channel estimation procedure for user k in RIS-assisted THz MIMO systems is summarized in Algorithm 1, where we integrate Phase 2 and Phase 3 together for simplicity.

B. Narrow Beams Design in Stage S

Given N bottom-stage narrow beams that covers the whole space, the AoA and AoD of a link is estimated by the central direction of the resulting narrow-beam pair. However, given a propagation path with arbitrary continuous angle φ^* in practice, the estimation by these finite and discrete directions leads to quantization error. In this subsection, we first define the codeword and the coverage of narrow beams. Then, we study the direction distribution design of these narrow beams for covering whole space.

For a terminal with N_a elements, the n th ARAP-based narrow-beam codeword in direction φ_n is simply given as $\mathbf{a}_{N_a}^S(\varphi_n)$ (see (10)). The normalized beam power of $\mathbf{a}_{N_a}(\varphi)$ in the direction ψ is given as

$$A(\mathbf{a}_{N_a}(\varphi), \psi) = \left| \mathbf{a}_{N_a}(\varphi)^H \mathbf{a}_{N_a}(\psi) \right| = \left| \frac{1}{N_a} \sum_{n=1}^{N_a} e^{jkd_a(n-1)[\sin(\psi) - \sin(\varphi)]} \right| \leq 1, \quad (24)$$

and we denote the beam coverage of $\mathbf{a}_{N_a}(\varphi)$ as

$$\mathcal{CV}(\mathbf{a}_{N_a}(\varphi)) = \{\psi \mid A(\mathbf{a}_{N_a}(\varphi), \psi) \geq \rho\} \quad (25)$$

where ρ is the coverage-edge energy, and the length of coverage is named as beam width hereafter. To design the direction distribution of narrow beams for covering whole space, it is important to understand the following lemma.

Lemma 1: Narrow beam in direction φ is equivalent to that in direction $\pi - \varphi$ in terms of terminal, i.e.,

$$\mathbf{a}_{N_a}(\varphi) = \mathbf{a}_{N_a}(\pi - \varphi). \quad (26)$$

Besides, the beam coverage of $\mathbf{a}_{N_a}(\varphi)$ is front-back mirror symmetrical about the array plane.

Proof: It is easy to verify that $\mathbf{a}_{N_a}(\varphi) = \mathbf{a}_{N_a}(\pi - \varphi)$. According to (24), we have $A(\mathbf{a}_{N_a}(\varphi), \psi) = A(\mathbf{a}_{N_a}(\varphi), \pi - \psi)$, i.e., $\mathcal{CV}(\mathbf{a}_{N_a}(\varphi)) = \pi - \mathcal{CV}(\mathbf{a}_{N_a}(\varphi))$. In general, the angle perpendicular to the plane is defined as 0 and the front range is $[-\pi/2, \pi/2]$. Thus, the beam coverage is front-back mirror symmetrical about array plane. ■

According to Lemma 1, beams with front-back mirror symmetry about array plane are isomorphic. For simplicity of exposition hereafter, we use the same notation φ_i for a pair of front-back symmetrical beam. Considering half-wavelength

Algorithm 1: Cooperative Channel Estimation Procedure for User k in RIS-assisted THz MIMO Systems.

Input: The RIS allocation set $\mathbb{L}(k)$, number of narrow beams N ; hierarchical codebook $\{\omega_n^s\}_{s=1}^S$, $S = \log_3^N$.
Initialization: $D_k = \text{card}[\mathbb{L}(k)] + 1$.
Phase 1:
for $p = 1 : 3$ **do**
 BS uses precoder ω_p^1 .
 for $q = 1 : 3$ **do**
 User k uses combiner ω_q^1
 for $i = 1 : N$ **do**
 All RIS l ($l \in \mathbb{L}(k)$) turn to $\Theta_{\text{ref}}(-2 + \frac{4i-2}{N})$.
 if user k detects a pulse with identity l . **then**
 Output result: $\Delta_{l,k} = -2 + \frac{4i-2}{N}$.
Phase 2 and Phase 3:
for Path $L = 1 : D_k$ **do**
 if $L = 1$ **then**
 Shut down all RISs.
 else
 Fix all RIS l ($l \in \mathbb{L}(k)$) in $\Theta_{\text{ref}}(\Delta_{l,k})$
 for $p = 1 : 3$ **do**
 BS uses precoder ω_p^1 .
 for $q = 1 : 3$ **do**
 User k uses combiner ω_q^1 .
 $\mathbf{y}_s^{\text{Ues}} = \sqrt{P} \text{vec}(\mathbf{Q}_s^H \mathbf{H}_k \mathbf{P}_s + \mathbf{N}_{\text{noise}})$.
 if $L \geq 2$ **then**
 $\mathbf{y}_s^{\text{Ues}} = \mathbf{y}_s^{\text{Ues}} - \sum_{n=1}^{L-1} \sqrt{P} G_t G_r a_{\text{path}}^n \mathbf{Q}_s^H \mathbf{m}_q^n (\mathbf{m}_p^n)^H \omega_{p_1^*}^1$.
 $n^* = \arg \max_n [\mathbf{y}_s^{\text{Ues}} \odot (\mathbf{y}_s^{\text{Ues}})^\dagger](n)$,
 $p_1^* = \lfloor n^*/3 \rfloor$ and $q_1^* = \text{mod}_3(n^*)$.
 /* Hierarchical search on user k side */
 for Stage $s = 2 : S$ **do**
 BS uses precoder $\omega_{p_1^*}^s$.
 for $q = 3q_{s-1}^* - 2 : 3q_{s-1}^*$ **do**
 User k uses combiner ω_q^s .
 $\mathbf{y}_s^{\text{Ues}} = \sqrt{P} \mathbf{Q}_s^H \mathbf{H}_k \omega_{p_1^*}^s + \mathbf{n}$.
 if $L \geq 2$ **then**
 $\mathbf{y}_s^{\text{Ues}} = \mathbf{y}_s^{\text{Ues}} - \sum_{n=1}^{L-1} \sqrt{P} G_t G_r a_{\text{path}}^n \mathbf{Q}_s^H \mathbf{m}_q^n (\mathbf{m}_p^n)^H \omega_{p_1^*}^s$.
 $q_s^* = 3q_{s-1}^* + \arg \max_n [\mathbf{y}_s^{\text{Ues}} \odot (\mathbf{y}_s^{\text{Ues}})^\dagger](n)$.
 /* Hierarchical search on BS side */
 for Stage $s = 2 : S$ **do**
 User k uses precoder $\omega_{q_s^*}^s$.
 for $p = 3p_{s-1}^* - 2 : 3p_{s-1}^*$ **do**
 BS uses combiner ω_p^s .
 $\mathbf{y}_s^{\text{Bes}} = \sqrt{P} \mathbf{P}_s^H \mathbf{H}_k^T \omega_{q_s^*}^s + \mathbf{n}$.
 if $L \geq 2$ **then**
 $\mathbf{y}_s^{\text{Bes}} = \mathbf{y}_s^{\text{Bes}} - \sum_{n=1}^{L-1} \sqrt{P} G_t G_r a_{\text{path}}^n \mathbf{P}_s^H (\mathbf{m}_p^n)^\dagger (\mathbf{m}_q^n)^T \omega_{q_s^*}^s$.
 $p_s^* = 3p_{s-1}^* + \arg \max_n [\mathbf{y}_s^{\text{Bes}} \odot (\mathbf{y}_s^{\text{Bes}})^\dagger](n)$.
 $\mathbf{m}_p^L = \omega_{p_s^*}^S$, $\mathbf{m}_q^L = \omega_{q_s^*}^S$, $a_{\text{path}}^L = |\mathbf{y}_s^{\text{Bes}}(n_s^*) / \sqrt{P} G_t G_r|$.
Output result: Pathloss a_{path}^L , AoD and AoA of path L and the direction of \mathbf{m}_p^L and \mathbf{m}_q^L .

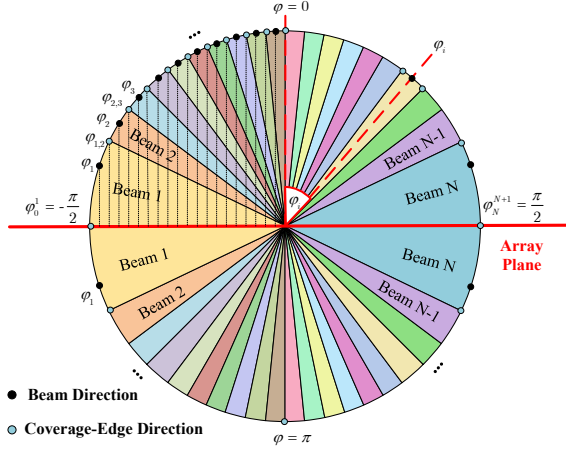


Fig. 9. Narrow-beam patterns in different directions with common ρ .

antenna spacing, we have the following Proposition and Corollary for narrow beams' direction distribution design.

Proposition 1: For N ($N \geq N_a$) narrow beams covering all directions with common ρ , we use $\{\varphi_i\}_{i=1}^N$ to represent the i th beam direction and $\{\varphi_i^{i\pm 1}\}_{i=1}^N$ to represent the coverage-edge direction of i th beam. As shown in Fig. 9, to satisfy common ρ , each beam yields different beam width. For \forall i th beam, we have

$$|\sin \varphi_i^{i+1} - \sin \varphi_i| = |\sin \varphi_i - \sin \varphi_i^{i-1}| = \frac{1}{N} \quad (27)$$

and

$$\rho = \frac{\sin[(N_a \pi)/2N]}{N_a \sin[\pi/2N]}, \quad (28)$$

where ρ is monotonically increasing with the increase of N when $N \geq N_a$. The beam direction of $\{\varphi_i\}_{i=1}^N$ is given as

$$\varphi_i = \begin{cases} \arcsin \left[\frac{2i-1}{N} - 1 \right], & \text{front range (FR)} \\ \pi - \arcsin \left[\frac{2i-1}{N} - 1 \right], & \text{back range (BR)} \end{cases}. \quad (29)$$

Corollary 1:² Suppose the same beam width $\Delta\varphi = \pi/N$ for N ($N \geq N_a$) is defined for uniformly distributed narrow beams such as

$$\mathbf{a}_{N_a}(\varphi_i) \Big|_{\varphi_i} = \begin{cases} -\frac{\pi}{2} + \frac{(2i-1)\pi}{2N}, & \text{FR} \\ \frac{3\pi}{2} - \frac{(2i-1)\pi}{2N}, & \text{BR} \end{cases} \quad (30)$$

for $i = 1, \dots, N$ with

$$\mathcal{CV}(\mathbf{a}_{N_a}(\varphi_i)) = \begin{cases} \left[-\frac{\pi}{2} + \frac{(i-1)\pi}{N}, -\frac{\pi}{2} + \frac{i\pi}{N} \right], & \text{FR} \\ \left[\frac{3\pi}{2} - \frac{i\pi}{N}, \frac{3\pi}{2} - \frac{(i-1)\pi}{N} \right], & \text{BR} \end{cases}. \quad (31)$$

ρ is various for different beams and is lower bounded by a function of $\Delta\varphi$ for all beams as

$$\rho > \frac{\sin[(\Delta\varphi N_a \pi)/4]}{N_a \sin[(\Delta\varphi \pi)/4]}. \quad (32)$$

²The beam width is referred to the width of one side.

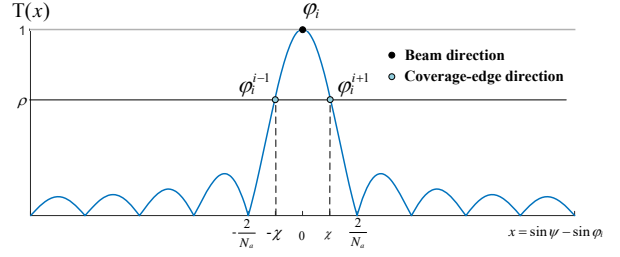


Fig. 10. Normalized i th beam power distribution in different directions.

Proof: For narrow beam in direction φ , the normalized beam power in (24) can be further expressed as

$$\begin{aligned} A(\mathbf{a}_{N_a}(\varphi), \psi) &= \left| \frac{1}{N_a} \sum_{n=1}^{N_a} e^{j k d_a (n-1) [\sin(\psi) - \sin(\varphi)]} \right| \\ &= \left| \frac{1}{N_a} \frac{e^{j \frac{N_a k d_a m}{2}} \left(e^{j \frac{N_a k d_a m}{2}} - e^{-j \frac{N_a k d_a m}{2}} \right)}{e^{j \frac{k d_a m}{2}} \left(e^{j \frac{k d_a m}{2}} - e^{-j \frac{k d_a m}{2}} \right)} \right| \\ &= \left| \frac{1}{N_a} e^{j \frac{(N_a-1) k d_a m}{2}} \frac{\sin[(N_a k d_a m)/2]}{\sin[(k d_a m)/2]} \right|, \end{aligned}$$

where $m = \sin(\psi) - \sin(\varphi)$. Thus, for half-wavelength antenna spacing, i.e., $d_a = \lambda/2$, the normalized beam power of $\mathbf{a}_{N_a}(\varphi_i)$ is given as

$$A(\mathbf{a}_{N_a}(\varphi_i), \psi) = \left| \frac{\sin[\frac{N_a \pi}{2} (\sin(\psi) - \sin(\varphi_i))]}{N_a \sin[\frac{\pi}{2} (\sin(\psi) - \sin(\varphi_i))]} \right|. \quad (33)$$

Define a function $T(x) = |\sin(\frac{N_a \pi}{2} x) / [N_a \sin(\frac{\pi}{2} x)]|$. As shown in Fig. 10, it can be observed that the beam power is monotonically decreasing with the increase of $|x|$ when $|x| \leq 2/N_a$. Thus, the common ρ yields common $|x|$ for all beams, and for \forall i th beam, we have

$$|\sin \varphi_i^{i+1} - \sin \varphi_i| = |\sin \varphi_i - \sin \varphi_i^{i-1}| = \chi(\rho), \quad (34)$$

where χ is a constant and subjected to the inverse function of $\rho = T(\chi)$. When all the N beams cover all directions as shown in Fig. 9, we have $2N$ of χ uniformly divide the interval $[-1, 1]$ with $\chi = 1/N$ and the condition $N \geq N_a \Rightarrow \chi < 1/N_a$. Thus, ρ is monotonically increasing with the increase of N . In Fig. 9, $\sin \varphi_1, \dots, \sin \varphi_N$ uniformly divides the interval $[-1, 1]$ and it is easy to obtain the beam direction by combining the feasible domain of the arcsine function.

Before proving corollary 1, we first provide a key lemma which serves as the basis of the derivations that follows.

Lemma 2: Given two angle directions φ_1 and φ_2 , we have following relation that

$$\begin{aligned} |\sin \varphi_1 - \sin \varphi_2| &= \left| 2 \cos \frac{\varphi_1 + \varphi_2}{2} \sin \frac{\varphi_1 - \varphi_2}{2} \right| \\ &\leq 2 \left| \sin \frac{\varphi_1 - \varphi_2}{2} \right| \stackrel{(a)}{<} |\varphi_1 - \varphi_2|, \end{aligned} \quad (35)$$

where (a) comes from $|\sin x| < |x|$ on condition that $|x| > 0$.

For beams with the same beam width, the i th beam direction and coverage-edge direction in FR is given as

$$\varphi_i = \frac{2i-1-\pi}{2N}, \quad \varphi_i^{i-1} = \frac{(2i-2-N)\pi}{2N}, \quad \varphi_i^{i+1} = \frac{(2i-N)\pi}{2N},$$

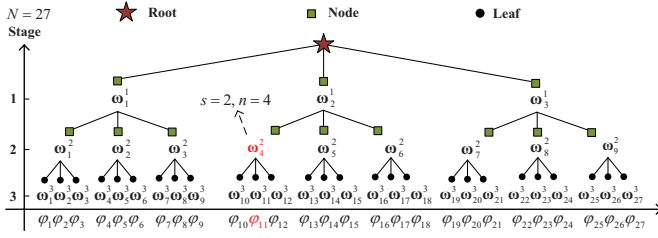


Fig. 13. Beam candidates of 3-tree hierarchical scheme when $S \geq 3$.

sub-optimally accomplished by solving a classical minimum Euclidean distance problem as

$$\{\mathbf{F}_{RF}, \mathbf{f}_B^{s,n}\} = \arg \min \|\omega_n^s - \mathbf{F}_{RF} \mathbf{f}_B^{s,n}\|_F \quad (43a)$$

$$\text{s.t.} \quad \|\mathbf{F}_{RF} \mathbf{f}_B^{s,n}\| = 1, \quad (43b)$$

$$|\mathbf{F}_{RF}(:, i)| \in \mathcal{F}_{RF}, \quad \forall i. \quad (43c)$$

Problem (43) has been extensively studied and the orthogonal matching pursuit (OMP) algorithm can be applied to it [17]. It is worth noting that the approximate/sub-optimal solutions in (42) and (43) would result in double-stage error and each wide beam realization requires all RF chains by TD approach. Therefore, in the following, we additionally propose a PSD approach to design wide beams for 3-tree search, by which only one RF chain is needed for each wide beam realization and multi-beams can be simultaneously utilized to reduce search time. The core concept of PSD approach is to let each RF chain control a subset of antennas by deactivating some phase shifters on the ARAP-based narrow beam codeword, so as to further form wide beam via less active antenna number. Now, we propose the following Criterion for the PSD-based wide beams design to complete the 3-tree codebook.

Criterion 4: By PSD approach in 3-tree search, each RF chain occupies 3^s adjacent antennas to form beam vector in stage $s = 1, \dots, s_{\max}$, where $s_{\max} = \lfloor \log_3 N_a \rfloor$. In stage $s = s_{\max} + 1, \dots, S$, all N_a antennas are used to form beam vector. Thus, the n th beam codeword in stage s can be expressed as

$$\omega_n^s = \begin{cases} \mathbf{a}_{3^s}(\varphi_{i(N,n,s)}), & s = 1, \dots, s_{\max} \\ \mathbf{a}_{N_a}(\varphi_{i(N,n,s)}), & s = s_{\max} + 1, \dots, S \end{cases}, \quad (44)$$

in which $n = 1, \dots, 3^s$,

$$i(N, n, s) = \frac{N \cdot 3^{-s}(2n - 1) + 1}{2} \quad (45)$$

and the definition of φ_i is same as the definition in (39). For easier understanding of (45), we present an example direction distribution map in Fig. 13 with respect to $N = 27$. In case of $N_a \geq 9$, via (44) and (45), we reach

$$\omega_4^2 = \mathbf{a}_9(\varphi_{11}),$$

the direction φ_i of which can be directly obtained from the direction distribution map (red one in Fig. 13).

Proposition 3: Based on PSD in Criterion 4, the wide beams have common coverage-edge energy ρ . To cover whole space, the $\rho(s)$ of ω_n^s in s stage is given as

$$\rho(s) = \begin{cases} \frac{1}{3^s \sin\left(\frac{\pi}{2 \cdot 3^s}\right)}, & s = 1, \dots, s_{\max} \\ \frac{\sin\left(\frac{N_a \pi}{3^s}\right)}{N_a \sin\left(\frac{\pi}{2 \cdot 3^s}\right)}, & s = s_{\max} + 1, \dots, S \end{cases}. \quad (46)$$

As such, the coverage of the union of three beams in the next stage is exactly the same as that of the ω_n^s , i.e.,

$$\mathcal{CV}(\omega_n^s) = \mathcal{CV}(\omega_{3n-2}^{s+1}) \cup \mathcal{CV}(\omega_{3n-1}^{s+1}) \cup \mathcal{CV}(\omega_{3n}^{s+1}). \quad (47)$$

Proof: The proofs are referred to Appendix B. ■

IV. DESIGN OF RISS AND HYBRID PRECODER/COMBINERS

Thanks to the natural sparsity of THz channels (see (6)) that are constructed by AoD and AoA vectors at both sides, we can steer the analog beam vectors pointing to these AoDs/AoAs in analog domain of transceivers and using digital precoder for power allocation [22]–[30]. We use $\hat{\varphi}_{B,M}^l, \hat{\varphi}_{B,H}^k, \hat{\varphi}_{U,H}^k, \hat{\varphi}_{U,N}^{l,k}$ to represent the estimated quantized angles. As a result, the design of RISSs serving for user k are given as

$$\Theta_l = \Theta_{\text{ref}}(\Delta_{l,k}), \quad l \in \mathbb{L}(k). \quad (48)$$

The design of analog precoder of BS and analog combiner of user k are given as

$$\begin{aligned} \mathbf{F}_{RF} &= \left[\mathbf{a}_{N_t}^B(\hat{\varphi}_{B,H}^1), \mathbf{a}_{N_t}^B(\hat{\varphi}_{B,M}^{l_1^1}), \dots, \mathbf{a}_{N_t}^B(\hat{\varphi}_{B,M}^{l_{D_1-1}^1}), \right. \\ &\quad \mathbf{a}_{N_t}^B(\hat{\varphi}_{B,H}^2), \mathbf{a}_{N_t}^B(\hat{\varphi}_{B,M}^{l_1^2}), \dots, \mathbf{a}_{N_t}^B(\hat{\varphi}_{B,M}^{l_{D_2-1}^2}), \\ &\quad \dots, \\ &\quad \left. \mathbf{a}_{N_t}^B(\hat{\varphi}_{B,H}^K), \mathbf{a}_{N_t}^B(\hat{\varphi}_{B,M}^{l_1^K}), \dots, \mathbf{a}_{N_t}^B(\hat{\varphi}_{B,M}^{l_{D_K-1}^K}) \right] \\ \mathbf{W}_{RF}^k &= \left[\mathbf{a}_{N_u}^B(\hat{\varphi}_{U,H}^k), \mathbf{a}_{N_u}^U(\hat{\varphi}_{U,N}^{l_1^k}), \mathbf{a}_{N_u}^U(\hat{\varphi}_{U,N}^{l_2^k}), \right. \\ &\quad \dots, \mathbf{a}_{N_u}^U(\hat{\varphi}_{U,N}^{l_{(D_k-1)}^k}) \left. \right], \end{aligned} \quad (49)$$

where $l_1^k, l_2^k, \dots, l_{D_k-1}^k \in \mathbb{L}(k)$ denote the serial numbers of RISSs serving for user k . Next, a key lemma is introduced to provide the basis of the derivations that follows.

Lemma 3 ([53]): For a ULA system with azimuth angles of arrival or departure drawn independently from a continuous distribution, the transmit and receive array response vectors are orthogonal, i.e., we have $\mathbf{a}(\phi^k) \perp \text{span}(\{\mathbf{a}(\phi^l) | \forall l \neq k\})$ as the number of antenna elements, N_a , tends to infinity.

Lemma 3 indicated that when AoA/AoD of propagation links are different, massive MIMO channels yield space asymptotic orthogonal property as N_a turns infinity.

A. Digital Precoder/Combiners Design for Single-user Case

Consider a single user k , which means other users are passive. Depending on Lemma 3, we can directly use the digital precoder of BS to allocate power on these links. Such a direct allocation (DA) design can be written as

$$\mathbf{F}_B^k = \text{diag}\left(\sqrt{S_1}, \sqrt{S_2}, \dots, \sqrt{S_{D_k}}\right), \quad \mathbf{W}_B^k = \mathbf{I}. \quad (51)$$

where $\{S_i\}_{i=1}^{D_k}$ are the power allocation factors. As a result, the spectral efficiency of user k is degraded as

$$\begin{aligned} R_k &= \log_2 \det \left[\mathbf{I}_{D_k} + \frac{P}{\sigma_n^2} \mathbf{W}_k^H \mathbf{H}_k \mathbf{F}_k \mathbf{F}_k^H \mathbf{H}_k^H \mathbf{W}_k \right] \\ &= \log_2 \det \left[\mathbf{I}_{D_k} + \frac{P}{\sigma_n^2} \mathbf{F}_k^H \mathbf{H}_k^H \mathbf{H}_k \mathbf{F}_k \right] \\ &= \log_2 \det \left[\mathbf{I}_{D_k} + \frac{P}{\sigma_n^2} \mathbf{F}_k^H \text{diag}(\mathbf{a}_{\text{loss}}) \mathbf{F}_k \right], \end{aligned} \quad (52)$$

where $\mathbf{F}_k = \mathbf{F}_{RF} \mathbf{F}_B^i$ is the effective precoder component for k th user and \mathbf{a}_{loss} is the pathloss vector. The remaining objective of BS is to determine the power factor on these subchannels for maximizing the efficiency of user k , i.e.,

$$\begin{aligned} \max_{S_i} \log \prod_{i=1}^{D_k} 1 + \frac{P}{\sigma_n^2} \mathbf{a}_{\text{loss}}(i)^2 S_i \\ \text{s.t.} \quad \sum_{i=1}^{D_k} S_i = 1, \quad \{S_i\}_{i=1}^{D_k} \geq 0. \end{aligned} \quad (53)$$

Problem (53) admits a convex form of the classic water-filling problem and the optimal solution can be obtained by resorting to the Karush-Kuhn-Tucker method, which is given by

$$S_i = \left[\frac{1}{\ln 2 \cdot \mu} - \frac{\sigma_n^2}{P \mathbf{a}_{\text{loss}}(i)^2} \right]^+, \quad i = 1, \dots, D_k, \quad (54)$$

where $[\cdot]^+ = \max\{\cdot, 0\}$. The Lagrange parameter $\mu > 0$ is chosen by 1-D search to satisfy the constraint $\sum_{i=1}^{D_k} S_i = 1$.

B. Digital Precoder/Combiners Design for Multi-user Case

For the case that multi users communicate simultaneously, the spectral efficiency of the k th user is given as [14]

$$R_k = \log_2 \det [\mathbf{I}_{N_u} + P \mathbf{W}_k \mathbf{C}_k^{-1} \mathbf{W}_k^H \mathbf{H}_k \mathbf{F}_k \mathbf{F}_k^H \mathbf{H}_k^H], \quad (55)$$

where $\mathbf{C}_k = P \mathbf{W}_k^H \mathbf{H}_k \left(\sum_{i \neq k} \mathbf{F}_i \mathbf{F}_i^H \right) \mathbf{H}_k^H \mathbf{W}_k + \sigma_n^2 \mathbf{W}_k^H \mathbf{W}_k$ is the covariance of effective interference plus noise at k th user. In this case, the intuitive strategy is to use the DA design directly for the overall links. However, inter-user interference can not be eliminated since these links are nearly orthogonal with finite massive antennas. With the increase of transmitted power, the inter-user interference will greatly reduce the total spectrum efficiency. Thus, at the high SNR regime, if N_a is not large enough, the performance of DA is degraded, as will be shown in Section VI.

To make up for the weakness of DA, we additionally propose a strategy that utilize the digital domain of BS to eliminate the inter-user interference. First, the effective channel of user k can be written as

$$\mathbf{H}_{\text{eff},k} = G_t G_r (\mathbf{W}_{RF}^k)^H \times \underbrace{[\mathbf{W}_{RF}^k \text{diag}(\mathbf{a}_{\text{loss}}) \mathbf{F}_{RF}^H(:, E_{k-1} + 1 : E_k)]}_{\text{estimated channel for user } k} \mathbf{F}_{RF}. \quad (56)$$

where $E_k = \sum_{i=1}^K D_k$ and $[:, E_{k-1} + 1 : E_k]$ represents columns $E_{k-1} + 1$ to E_k . Then, we formulate the zero-interference part of each effective channel by the block diagonalization (BD) approach [56]. For user k , concatenate the other effective channels as

$$\bar{\mathbf{H}}_{\text{eff},k} = [\mathbf{H}_{\text{eff},1}^T, \dots, \mathbf{H}_{\text{eff},k-1}^T, \mathbf{H}_{\text{eff},k+1}^T, \dots, \mathbf{H}_{\text{eff},K}^T]^T. \quad (57)$$

Using the singular value decomposition (SVD)

$$\bar{\mathbf{H}}_{\text{eff},k} = \bar{\mathbf{U}}_k \bar{\Sigma}_k [\bar{\mathbf{V}}_k^{\text{eff}}, \bar{\mathbf{V}}_k^{\text{zero}}]^H, \quad (58)$$

we obtain the null-space orthogonal basis of the other effective channels, which are the last $(N_t - D_k)$ right singular vectors, i.e., $\bar{\mathbf{V}}_k^{\text{zero}}$. Thus, the zero-interference part of $\bar{\mathbf{H}}_{\text{eff},k}$ can be written as $\mathbf{H}_k \bar{\mathbf{V}}_k^{\text{zero}}$. In this case, the digital precoder/combiners design with respect to $\mathbf{H}_k \bar{\mathbf{V}}_k^{\text{zero}}$ can be

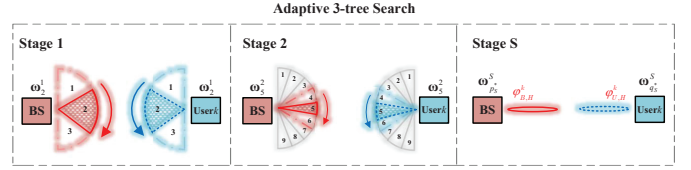


Fig. 14. An example of adaptive 3-tree hierarchical search scheme.

considered as the classic point-point MIMO design, and the optimal solution is given by the SVD with water-filling, i.e.,

$$\mathbf{H}_k \bar{\mathbf{V}}_k^{\text{zero}} = [\mathbf{U}_k^{\text{eff}}, \mathbf{U}_k^{\text{zero}}] \begin{bmatrix} \Sigma_k & \mathbf{0} \\ \mathbf{0} & \mathbf{0} \end{bmatrix} [\mathbf{V}_k^{\text{eff}}, \mathbf{V}_k^{\text{zero}}]^H, \quad (59)$$

in which $\mathbf{U}_k^{\text{eff}}$ (resp. $\mathbf{V}_k^{\text{eff}}$) represents the first D_k left (resp. right) singular vectors. Σ_k is a diagonal matrix that contains D_k elements representing the zero-interference-path gains. Thus, such a zero-forcing allocation (ZFA) design can be written as

$$\begin{aligned} \mathbf{F}_B^k &= \bar{\mathbf{V}}_k^{\text{zero}} \mathbf{V}_k^{\text{eff}} \text{diag}(\sqrt{S_{E_{k-1}+1}}, \sqrt{S_{E_{k-1}+2}}, \dots, \sqrt{S_{E_k}}), \\ \mathbf{W}_B^k &= \mathbf{U}_k^{\text{eff}}, \end{aligned} \quad (60)$$

where the overall links power allocation (S_1, \dots, S_{N_s}) at BS is obtained by water-filling on overall paths $\{\Sigma_k\}_{k=1}^K$.

V. DISCUSSION AND EXTENSIONS

In this section, several discussions and possible extension of the proposed framework will be briefly presented.

A. Discussion on Channel Estimation Procedure

Apart from the contribution to RIS-related cooperative procedure, we note that the concept of the proposed tree-search manner in Section III-A is inherently different from the traditional adaptive M -tree search in THz systems [4] or in mmWave systems [49]. The traditional adaptive M -tree search realizes the estimation by selecting beam pairs stage by stage with decreasing beam width on both side (see Fig. 14). In each stage, the user k determines the best one among $M \times M$ pairs and then feedback the pair information to BS. Thus, such a procedure needs S feedbacks, which is much more time consuming than search, and the total search time is given as

$$T_{\text{ad}} = M^2 \log_M^N. \quad (61)$$

In our procedure, we first search the narrow beam on user k side and then focus on the BS side. Regardless of the alignment step which needs one feedback, the whole procedure proposed needs no feedback for DA design. The total search time is given as

$$T_{\text{new}} = M \log_M^N + M \log_M^N = 2M \log_M^N, \quad (62)$$

and we have $T_{\text{new}} \leq T_{\text{ad}}$ since $M \geq 2$. To estimate the $2D_k - 1$ RIS-assisted channels for user k , the total number of steps needed by the proposed Algorithm 1 is $9N + D_k(3 + 6 \log_3^N)$. If 3 chains are used in the MS to combine the measurements by PSD codebook, the required number of search steps is then reduced to be $3N + D_k(1 + 2 \log_3^N)$.

B. Discussion on Hierarchical Codebook

We mention that the proposed TD approach is based on prior works [49]–[51] that happen to have the similar concept but the direction of their bottom-stage beams are uniformly distributed, which results in misalignment due to the different coverage-edge energy (see Corollary 1 and Proposition 2). Besides, the narrow beam number must satisfy $N = M^{n \in \mathbb{N}^+}$. To overcome above shortcomings, we first define the beam with common coverage-edge energy into the bottom stage (see (40)). For arbitrary N , Criterion 3 is proposed based on leaves in perspective of graph theory (unlike the principle based on uniform grid in above works). The proposed PSD approach is inspired by [22] which mentioned that wide beams can be formed by less antennas. We extend it into the HB architecture and standardize it into the 3-tree codebook.

C. Extension to the Planar RIS Case

For simplicity of exposition, the proposed estimation and beamforming framework is presented assuming ULA at the both sides of all link, which is catering for strip RIS in practice. We would like to point out that the basic design principle can be straightforwardly extended to the case of uniform planar array (UPA) by noting that the array response vector of a UPA can be represented as the Kronecker product of two ULA phase response vectors containing the angle pair (elevation and azimuth AoA/AoD) [4], [17]. Thus, the optimal solution to each RIS can be derived in closed form by AoA angle pair and AoD angel pair. The codewords of search mode in Section III-A can be obtained by sample N points on two-dimensional domain $[-2, 2] \times [-2, 2]$. The framework principle may even be applicable to circular and spherical arrays by decomposing their response vectors using Fourier series and spherical harmonics, respectively.

VI. SIMULATION RESULTS

In this section, we provide the simulation results to illustrate the performance of the proposed 3-tree codebooks for channel estimation and the performance of the proposed RISs and hybrid precoder/combiner solutions.

A. Performance of the Proposed Codebooks

In this subsection, we first evaluate the proposed narrow beams design by testing the misalignment rate, and the performance of the uniformly distributed narrow beams is included for comparison. Then, we study the beam patterns of the proposed 3-tree codebooks and evaluate their performance by testing final correct detection rate. As a benchmark, the traditional codebook in [49] which has the similar concept of the proposed TD codebook is presented.

Fig. 15 plots the misalignment rate (MR) versus SNR with different implementation parameters. As we can see, with the increase of SNR, the MR of our proposed narrow beams design gradually decreases to zero. In contrast, if uniformly distributed narrow beams are used for beam training, misalignment occurs even at high SNR regime. This observation verifies the *distribution rule* we provided in Proposition 3. These results also indicate that the minimum SNR that satisfies zero MR is related to the implementation parameters. It decreases with the increase of antenna number N_a and increases with the increase of narrow beam number N .

Fig. 16 illustrates the comparison of beam patterns by different approaches in the setting that $N_a = 32$ and $N = 81$, where the benchmark codebook and the TD codebook are the target

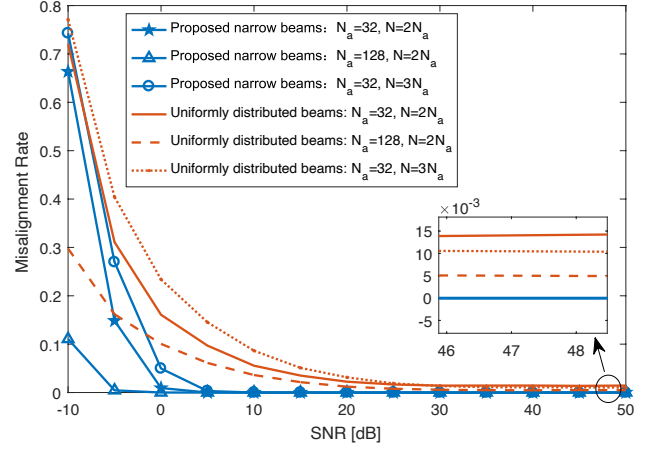


Fig. 15. Comparison of the misalignment rates between the proposed narrow beams design and uniformly distributed narrow beams.

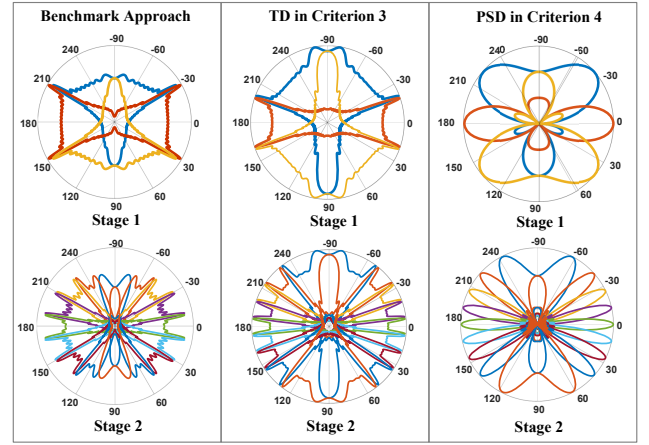


Fig. 16. Comparison of 3-tree beam patterns by benchmark codebook [49] and proposed codebooks where $N_a = 32$ and $N = 81$.

digital solutions as given in (42). For benchmark patterns, we observed that the beams width are identical on each side of array, e.g., $[-\pi/2, \pi/2]$, but have different coverage-edge energy. On the contrary, the beams by proposed approaches have common coverage-edge energy but different beam width. Comparing TD to PSD, we observe that the TD beams has better ability to suppress the energy in unintended range. Thus, while PSD codebook has the advantage of reduced search time, we speculate that the TD codebook shows better anti-noise performance.

For HB realization by the benchmark codebook and the TD codebook, we use the OMP algorithm in [17] to obtain HB solutions by (43) for both cases. In order to find the minimum number of RF chains needed to reach the target patterns in Fig. 16, we test the HB patterns in the second codebook stage by adding RF chains one by one in the simulation, and some of the test examples are demonstrated in Fig. 17. It is observed that while the benchmark codewords in second stage require 11 RF chains to approach to the target one, the TD codewords require only 5 RF chains.

Fig. 18 shows the comparison results of correct detection rate on single path. Comparing the TC upperbound and the benchmark upperbound, which are the performance of the target digital solutions, it is observed from Fig. 18 that the TC codebook significantly outperforms the benchmark codebook. Besides, using 14 RF chains in HB architecture,

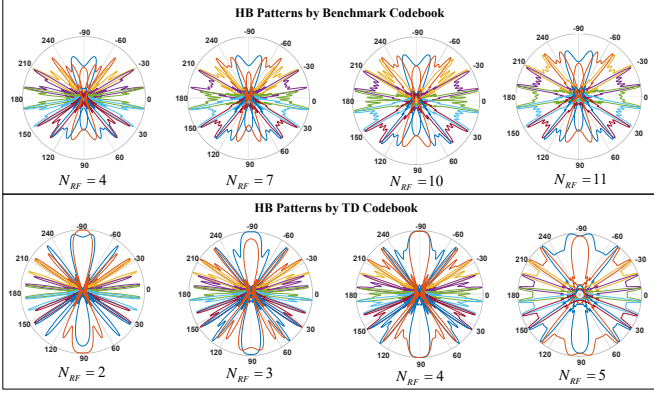


Fig. 17. HB patterns approximation of the codewords in the second codebook stage with different numbers of RF chains where $N_a = 32$ and $N = 81$.

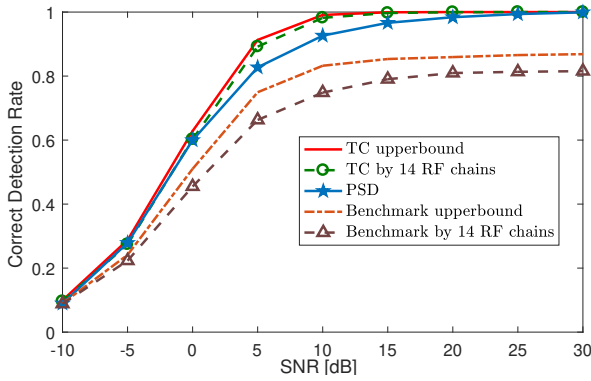


Fig. 18. Comparison of 3-tree search performance between different approaches where $N_a = 32$ and $N = 81$. The correct detection rate means the probability of successful alignment in all stages.

the performance of TC codebook approaches the upperbound but that of benchmark codebook does not. Comparing the performance between the proposed codebooks, we observed that the minimum SNR needed for TC codebook to achieve fully correct detection is lower than that of PSD, which proves our speculation on Fig. 16.

B. Performance of RISs and HB Design

In this subsection, we evaluate the performance of the transmission solutions. In order to highlight the main efficacy of the RISs for overcoming the LoS blockage problem, we consider such an indoor scenario that all LoS links between the BS and users are blocked by an obstacle as illustrated in Fig. 19, where BS is randomly located at $(0, d_B \in [0, 4])$ and $K = 3$ users are randomly located at $(0, d_{u_k} \in [4, 10])$. Six RISs are located at $(4, 2 + l)$ for $l = 1, \dots, 6$. The antenna spacing for all terminals is $d_a = \lambda/2$ and the active RISs reflection coefficient is $\beta = 1$. We consider the number of antennas/elements are identical $N_t = N_i = N_u = N_a$. The operating frequency is set to 0.3THz and the background noise power at the receiver is $\sigma_n^2 = -80\text{dBm}$. Absorption coefficient is $\tau(0.3T) = 0.0033/m$ and antenna gains are considered as $G_t = G_r = 10^{0.4} \sqrt{N_a}$. All the results presented were averaged over 10,000 random channel realizations. For comparison, we plot the following schemes.

- 1) *FDB with optimal RISs*: it is realized by the optimal RISs solution (12) and the SVD solution (single-user case) or zero-forcing solution (multi-user case).

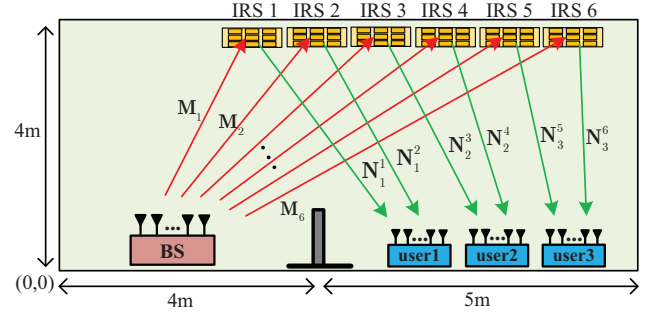


Fig. 19. The simulated RIS-assisted MIMO communication scenario.

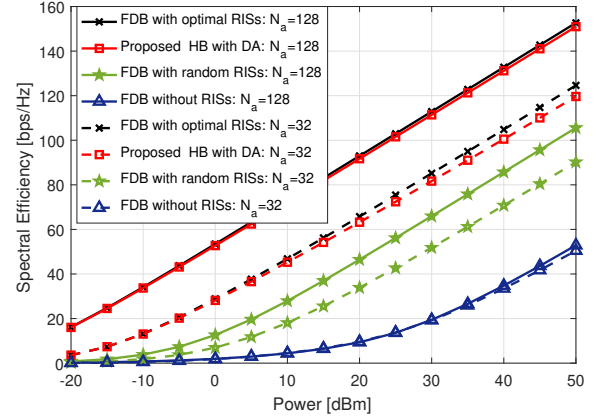


Fig. 20. Spectral efficiency versus transmit power for different schemes in single-user case where $N_t = N_i = N_u = N_a$ and $N_s = 6$.

- 2) *Proposed HB with DA*: it is realized by the proposed DA solutions and RISs solutions (single/multi-user case).
- 3) *Proposed HB with ZFA*: it is realized by the proposed ZFA solutions and RISs solutions (multi-user case).
- 4) *FDB with random RISs*: we randomly set the diagonal elements of Θ and then perform SVD solution (single user case) or zero-forcing solution (multi-user case).
- 5) *FDB without RISs*: In the case, we consider RISs as common wall, where the attenuations of first order rays are between 5.8 dB and 19.3dB compared to the LoS [55]. Thus, we set the matrix as $\Theta = \sqrt{0.1} \mathbf{I}_{N_r}$ (10dB) and then perform SVD solution (single-user case) or zero-forcing solution (multi-user case).

A. Single-user Case with Perfect CSI

We first evaluate the DA design with perfect CSI in single-user case, in which all six RISs serve one user. In this case, the FDB (SVD) with optimal RIS scheme is the capacity-achievable scheme. Fig. 20 plots the spectral efficiency versus transmit power at $N_a = 32$ and $N_a = 128$. It is seen that the performance gain of the RIS-assisted schemes is significant compared to the non-RIS-assisted benchmarks (random RIS and no RIS), since the LoS link is blocked and the reflecting links provide additional strong propagation paths. Moreover, as the number of antennas N_a increases from 32 to 128, the spectral efficiency achieved by the proposed HB with DA gets closer to the capacity, which validates the effectiveness of the proposed DA solutions in massive MIMO systems.

B. Multi-user Case with Perfect CSI:

Now, we evaluate the DA design and the ZFA design with perfect CSI in multi-user case, where the allocation set is $L(k) = \{l_k^1, l_k^2\}$ with $l_k^1 = 2k - 1$ and $l_k^2 = 2k$. In this case, the FDB (zero forcing) with optimal RIS scheme is almost

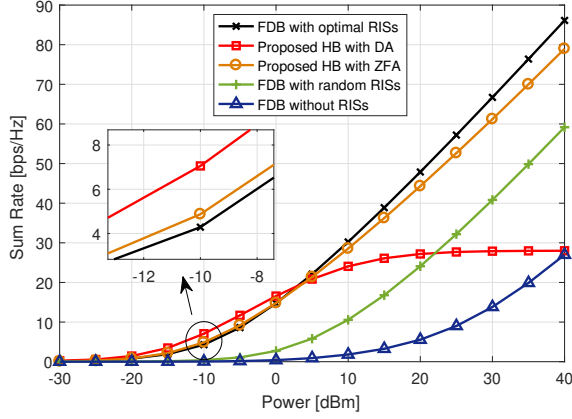


Fig. 21. Sum rate versus transmit power for different schemes in multi-user case where $N_t = N_i = N_u = 32$ and $N_s = 6$.

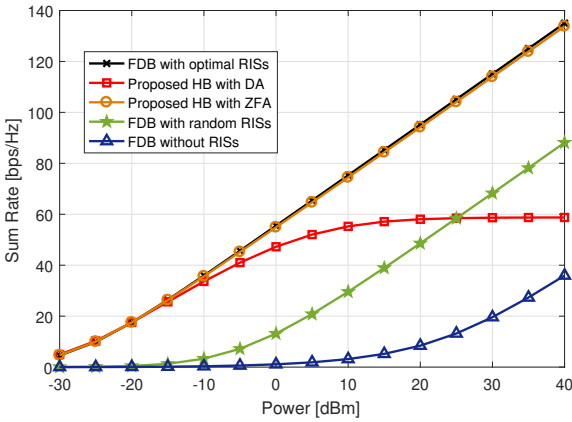


Fig. 22. Sum rate versus transmit power for different schemes in multi-user case where $N_t = N_i = N_u = 128$ and $N_s = 6$.

capacity-achievable at high SNR regime. Fig. 21 and Fig. 22 plot the sum rate versus transmit power at $N_a = 32$ and $N_a = 128$, respectively. Fig. 21 shows that the performance of DA design outperforms the zero-forcing benchmarks at low SNR regime with $N_a = 32$, and the performance of it is degraded at high SNR regime. This is because the user-interference largely reduces the overall spectral efficiency and its upper performance (at $\text{SNR} = +\infty$) is related to the beam orthogonality, i.e., subjected to N_a . Compared to Fig. 21, the performance of ZFA design in Fig. 22 is closer to that of FDB with optimal RISs. This can be explained as that the increase of N_a yields higher beam orthogonality which reduces the interference in analog domain, thus the HB with ZFA solution provides more zero-interference space for each user.

C. The Performance under Estimated CSI:

Finally, as shown in Fig. 23, we evaluate the performance of DA design and ZFA design under estimated CSI which is obtained by 3-tree codebook with N narrow-beam candidates. The gap between the performance under perfect CSI and that under estimated CSI is due to the AoAs/AoDs quantization error. With the increased estimation ratio N/N_a , the performance gap resulted from the quantization error decreases. It can be observed that the performance of the proposed designs are close to the FDB benchmark for the case $N_a = 32, N = 27$; $N_a = 32, N = 81$; $N_a = 64, N = 243$; and $N_a = 128, N = 243$. Thus, with large-scale antenna array implementation and adequate quantization resolution, the proposed framework exhibits comparable performance in the

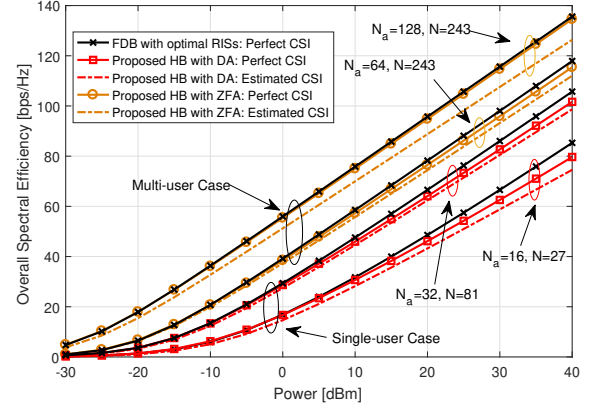


Fig. 23. The performance of DA design and ZFA design under estimated CSI which is obtained by 3-tree codebook with N narrow-beam candidates.

RIS-assisted MIMO system, with low hardware complexity ARAP-based HB architectures.

VII. CONCLUSION

We considered the channel estimation and transmission design for THz massive MIMO RIS-assisted system. Specifically, we proposed a cooperative channel estimation procedure via beam training, where three phases were developed to achieve different groups of measurements. To reduce search complexity, a 3-tree hierarchical search was adopted to realize the beam training. Then, we designed two novel codebooks for efficiently realizing the 3-tree search. As for narrow beams, we established the importance of designing these beams with common coverage-edge energy and we proposed a direction distribution rule. For wide beams design, tree dictionary (TD) approach and phase shifter deactivation (PSD) approach were proposed to complete the codebooks. Finally, we developed two closed-form transmission designs, i.e., direct allocation (DA) design and zero-forcing allocation (ZFA) design, for maximizing the overall spectral efficiency. Numerical results showed significant performance improvement of RIS-assisted schemes as compared to the non-RIS-assisted counterpart. Despite the low-complexity, the proposed HB solutions realizes spectral efficiency and sum rates that are comparable to FDB.

APPENDIX A PROOF OF (12)

The effective path gain can be rewritten as

$$\begin{aligned} & \left| \mathbf{a}_{N_r}^B \left(\varphi_{R,N}^{l,k} \right)^H \mathbf{\Theta}_l \mathbf{a}_{N_r}^R \left(\varphi_{R,M}^l \right) \right| \\ &= \frac{\beta}{N_r} \left| \sum_{n=1}^{N_r} e^{j[kd_a(n-1)(\sin \varphi_{R,M}^l - \sin \varphi_{R,N}^{l,k}) + \theta_n]} \right| \leq \beta, \end{aligned} \quad (63)$$

where the equality in (63) holds when

$$\theta_n = kd_a(n-1)(\sin \varphi_{R,N}^{l,k} - \sin \varphi_{R,M}^l) + a, \quad (64)$$

where a is an arbitrary constant and we let $a = 0$ in (12).

APPENDIX B PROOF OF PROPOSITION 3

According to Criterion 4, the active antenna number for each wide beam is $N_{\text{act}} = 3^s$ with respect to $s = 1, \dots, s_{\text{max}}$.

Let φ_n and φ_n^e denote the beam direction and coverage-edge direction of ω_n^s , we have

$$\left| \frac{\sin \left[\frac{N_{\text{act}} \pi}{2} \right] \sin \varphi_n - \sin \varphi_n^e}{N_{\text{act}} \sin \left[\frac{\pi}{2} \right] \sin \varphi_n - \sin \varphi_n^e} \right| \quad (65)$$

$$= \left| \frac{\sin \left[\frac{N_{\text{act}} \pi}{2} (\sin \varphi_n - \sin \varphi_n^e) \right]}{N_{\text{act}} \sin \left[\frac{\pi}{2} (\sin \varphi_n - \sin \varphi_n^e) \right]} \right|$$

$$= A(\mathbf{a}_{N_{\text{act}}}(\varphi_n), \varphi_n^e) = \rho(s) = \frac{1}{3^s \sin \left(\frac{\pi}{2 \cdot 3^s} \right)}$$

$$= \frac{\sin \left(\frac{3^s \pi}{2 \cdot 3^s} \right)}{3^s \sin \left(\frac{\pi}{2 \cdot 3^s} \right)} = \left| \frac{\sin \left(\frac{N_{\text{act}} \pi}{2 \cdot 3^s} \right)}{N_{\text{act}} \sin \left(\frac{\pi}{2 \cdot 3^s} \right)} \right|,$$

$$\Rightarrow |\sin \varphi_n - \sin \varphi_n^e| = \frac{1}{3^s}. \quad (66)$$

Consider the beam direction given in Criterion 4, by substituting (45) into (39), the beam direction is given as

$$\varphi_n = \begin{cases} \arcsin(3^{-s}(2n-1)-1), & \text{FR} \\ \pi - \arcsin(3^{-s}(2n-1)-1), & \text{BR} \end{cases} \quad (67)$$

From (66), we reach the coverage-edge direction as

$$\varphi_n^e = \begin{cases} \arcsin(3^{-s}(2n-1 \pm 1)-1), & \text{FR} \\ \pi - \arcsin(3^{-s}(2n-1 \pm 1)-1), & \text{BR} \end{cases} \quad (68)$$

Thus, the beam coverage of ω_n^s can be expressed as

$$\mathcal{CV}(\omega_n^s) = \begin{cases} [\arcsin(3^{-s}(2n-2)-1), \arcsin(3^{-s}2n-1)], & \text{FR} \\ \pi - [\arcsin(3^{-s}(2n-2)-1), \arcsin(3^{-s}2n-1)], & \text{BR} \end{cases} \quad (69)$$

It can be easily proved that (69) still holds for $s = s_{\max} + 1, \dots, \log_3^N$ in similar way. As a result, we reach

$$\mathcal{CV}(\omega_n^s) = \mathcal{CV}(\omega_{3n-2}^{s+1}) \cup \mathcal{CV}(\omega_{3n-1}^{s+1}) \cup \mathcal{CV}(\omega_{3n}^{s+1}). \quad (70)$$

REFERENCES

- [1] I. F. Akyildiz, J. M. Jornet, and C. Han, "Terahertz band: Next frontier for wireless communications," *Physical Communication (Elsevier)*, vol. 12, pp. 16-32, Sep. 2014.
- [2] S. Priebe and T. Krner, "Stochastic modeling of THz indoor radio channels," *IEEE Trans. Wireless Commun.*, vol. 12, no. 9, pp. 4445-4455, Sep. 2013.
- [3] J. M. Jornet and I. F. Akyildiz, "Channel modeling and capacity analysis for electromagnetic wireless nanonetworks in the Terahertz band," *IEEE Trans. Wireless Commun.*, vol. 10, no. 10, pp. 3211-3221, Oct. 2011.
- [4] C. Lin and G. Y. Li, "Indoor terahertz communications: How many antenna arrays are needed?" *IEEE Trans. Wireless Commun.*, vol. 14, no. 6, pp. 3097-3107, Jun. 2015.
- [5] C. Han, A. O. Bicen, and I. F. Akyildiz, "Multi-ray channel modeling and wideband characterization for wireless communications in the terahertz band," *IEEE Trans. Wireless Commun.*, vol. 14, no. 5, pp. 2402-2412, May 2015.
- [6] E. Larsson, et al., "Massive MIMO for next generation wireless systems," *IEEE Commun. Mag.*, vol. 52, no. 2, pp. 186-195, Feb. 2014.
- [7] M. Di Renzo et al. "Smart radio environments empowered by reconfigurable ai meta-surfaces: An idea whose time has come," *EURASIP J. Wireless Commun. Networking*, 2019. vol. 2019, no. 129, May 23 2019. doi: 10.1186/s13638-019-1438-9.
- [8] S. Sun, T. S. Rappaport, R. W. Heath, Jr., A. Nix, and S. Rangan, "MIMO for millimeter-wave wireless communications: Beamforming, spatial multiplexing, or both?" *IEEE Commun. Mag.*, vol. 52, no. 12, pp. 110-121, Dec. 2014.
- [9] A. Alkhateeb, J. Mo, N. Gonzalez-Prelcic, and R. W. Heath, Jr., "MIMO precoding and combining solutions for millimeter-wave systems," *IEEE Commun. Mag.*, vol. 52, no. 12, pp. 122-131, Dec. 2014.
- [10] L. Zhang et al., "Space-time-coding digital metasurfaces," *Nat. Commun.*, vol. 9, pp. 1-11, Oct. 2018.
- [11] T. J. Cui, M. Q. Qi, X. Wan, J. Zhao, and Q. Cheng, "Coding metamaterials, digital metamaterials and programmable metamaterials," *Light: Science & Applications*, vol. 3, no. 10, pp. e218, Oct. 2014.
- [12] S. Hu, F. Rusek, and O. Edfors, "Beyond massive MIMO: The potential of data transmission with large intelligent surfaces," *IEEE Trans. Signal Process.*, vol. 66, no. 10, pp. 2746-2758, May 2018.
- [13] X. Zhang, A. F. Molisch, and S.-Y. Kung, "Variable-phase-shift-based RF-baseband codesign for MIMO antenna selection," *IEEE Trans. Signal Process.*, vol. 53, no. 11, pp. 4091-4103, Nov. 2005.
- [14] F. Sohrabi and W. Yu, "Hybrid digital and analog beamforming design for large-scale antenna arrays," *IEEE J. Sel. Topics Signal Process.*, vol. 10, no. 3, pp. 501-513, Apr. 2016.
- [15] S. Payami, M. Ghorashi, and M. Dianati, "Hybrid beamforming for large antenna arrays with phase shifter selection," *IEEE Trans. Wireless Commun.*, vol. 15, no. 11, pp. 7258-7271, Nov. 2016.
- [16] L. Liang, W. Xu, and X. Dong, "Low-complexity hybrid precoding in massive multiuser MIMO systems," *IEEE Wireless Commun. Lett.*, pp. 653-656, 2014.
- [17] O. El Ayach et al., "Spatially sparse precoding in millimeter wave MIMO systems," *IEEE Trans. Wireless Commun.*, vol. 13, no. 2, pp. 1499-1513, Mar. 2014.
- [18] X. Yu, J.-C. Shen, J. Zhang, and K. B. Letaief, "Alternating minimization algorithms for hybrid precoding in millimeter wave MIMO systems," *IEEE J. Sel. Topics Signal Process.*, vol. 10, no. 3, pp. 485-500, Apr. 2016.
- [19] W. Ni, X. Dong, and W. S. Lu, "Near-optimal hybrid processing for massive MIMO systems via matrix decomposition," *IEEE Trans. Signal Process.*, vol. 65, no. 15, pp. 3922-3933, Aug. 2017.
- [20] J.-C. Chen, "Hybrid beamforming with discrete phase shifters for millimeter-wave massive MIMO systems," *IEEE Trans. Veh. Technol.*, vol. 66, no. 8, pp. 7604-7608, Aug. 2017.
- [21] J. Brady, N. Behdad, and A. M. Sayeed, "Beamspace MIMO for millimeter-wave communications: System architecture, modeling, analysis, and measurements," *IEEE Trans. Antennas Propag.*, vol. 61, no. 7, pp. 3814-3827, Jul. 2013.
- [22] T. He and Z. Xiao, "Suboptimal beam search algorithm and codebook design for millimeter-wave communications," *Mobile Netw. Appl.*, vol. 20, no. 1, pp. 86-97, Jan. 2015.
- [23] G. Zhu et al., "Hybrid beamforming via the kronecker decomposition for the millimeter-wave massive MIMO systems," *IEEE J. Sel. Areas Commun.*, vol. 35, no. 9, pp. 2097-2114, Sep. 2017.
- [24] J. Wang et al., "Beam codebook based beamforming protocol for multi-Gbps millimeter-wave WPAN systems," *IEEE J. Sel. Areas Commun.*, vol. 27, no. 8, pp. 1390-1399, Oct. 2009.
- [25] X. Gao, L. Dai, Y. Zhang, T. Xie, X. Dai, and Z. Wang, "Fast channel tracking for terahertz beamspace massive MIMO systems," *IEEE Trans. Veh. Technol.*, vol. 66, no. 7, pp. 5689-5696, Jul. 2017.
- [26] J. Zhao, F. Gao, W. Jia, S. Zhang, S. Jin, and H. Lin, "Angle domain hybrid precoding and channel tracking for millimeter wave massive MIMO systems," *IEEE Trans. Wireless Commun.*, vol. 16, no. 10, pp. 6868-6880, Oct. 2017.
- [27] L. Chen, Y. Yang, X. Chen, and W. Wang, "Multi-stage beamforming codebook for 60 GHz WPAN," in *Proc. 6th Int. ICST Conf. Commun. Netw. China (CHINACOM)*, Harbin, China, Aug. 2011, pp. 361-365.
- [28] Z. Xiao, T. He, P. Xia, and X.-G. Xia, "Hierarchical codebook design for beamforming training in millimeter-wave communication," *IEEE Trans. Wireless Commun.*, vol. 15, no. 5, pp. 3380-3392, May 2016.
- [29] Z. Xiao et al., "Enhanced Channel Estimation and Codebook Design for Millimeter-Wave Communication," *IEEE Trans. Veh. Technol.*, vol. 67, no. 10, pp. 9393-9405, Oct. 2018.
- [30] J. Zhang, Y. Huang, Q. Shi, J. Wang, and L. Yang, "Codebook design for beam alignment in millimeter wave communication systems," *IEEE Trans. Commun.*, vol. 65, no. 11, pp. 4980-4995, Nov. 2017.
- [31] X. Tan, Z. Sun, J. M. Jornet, and D. Pados, "Increasing indoor spectrum sharing capacity using smart reflect-array," in *Proc. IEEE ICC*, 2016, pp. 16.
- [32] X. Tan, Z. Sun, D. Koutsonikolas, and J. M. Jornet, "Enabling indoor mobile millimeter-wave networks based on smart reflect-arrays," in *Proc. IEEE INFOCOM*, 2018, pp. 270-278.
- [33] E. Basar et al., "Wireless communications through reconfigurable intelligent surfaces," *IEEE Access*, vol. 7, pp. 116753-116773, 2019.
- [34] C. Huang et al., "Achievable rate maximization by passive intelligent mirrors," in *Proc. IEEE ICASSP*, pp. 3714-3718, 2018.
- [35] C. Huang, G. C. Alexandropoulos, A. Zappone, M. Debbah, and C. Yuen, "Energy efficient multi-user MISO communication using low resolution large intelligent surfaces," in *Proc. IEEE GLOBECOM*, Abu Dhabi, UAE, Dec. 2018, pp. 1-6.
- [36] C. Huang, A. Zappone, G. C. Alexandropoulos, M. Debbah, and C. Yuen, "Reconfigurable Intelligent Surfaces for Energy Efficiency in Wireless Communication," *IEEE Trans. Wireless Commun.*, vol. 18, no. 8, pp. 4157-4170, Jun. 2019.
- [37] Q. Wu and R. Zhang, "Intelligent Reflecting Surface Enhanced Wireless Network: Joint Active and Passive Beamforming Design," in *Proc. IEEE GLOBECOM*, Abu Dhabi, UAE, Dec. 2018, pp. 1-6.
- [38] Q. Wu et al., "Intelligent reflecting surface enhanced wireless network via joint active and passive beamforming," *IEEE Trans. Wireless Commun.*, vol. 18, no. 11, pp. 5394-5409, Aug. 2019.

- [39] Q. Wu and R. Zhang, "Beamforming optimization for intelligent reflecting surface with discrete phase shifts," in *Proc. IEEE ICASSP, Brighton, UK*, May 2019, pp. 7830-7833.
- [40] Q.-U.-A. Nadeem *et al.*, "Large intelligent surface assisted MIMO communications," *arXiv:1903.08127*, 2019.
- [41] H. Guo *et al.*, "Weighted sum-rate optimization for intelligent reflecting surface enhanced wireless networks," *preprint arXiv:1905.07920*, 2019.
- [42] M. Cui, G. Zhang, and R. Zhang, "Secure wireless communication via intelligent reflecting surface," *IEEE Wireless Commun. Lett.*, vol. 8, no. 11, pp. 1410-1414, Oct. 2019.
- [43] B. Ning *et al.*, "Intelligent Reflecting Surface Design for MIMO System by Maximizing Sum-Path-Gains," *preprint arXiv:1909.07282*, 2019.
- [44] J. Ye, S. Guo, M. S. Alouini, "Joint Reflecting and Precoding Designs for SER Minimization in Reconfigurable Intelligent Surfaces Assisted MIMO Systems," *arXiv:1906.11466*, 2019.
- [45] S. Zhang and R. Zhang, "Capacity characterization for intelligent reflecting surface aided MIMO communication," *preprint arXiv:1910.01573*, 2019.
- [46] D. Mishra and H. Johansson, "Channel estimation and low-complexity beamforming design for passive intelligent surface-assisted MISO wireless energy transfer," in *Proc. IEEE Int. Conf. Acoustics Speech Signal Process. (ICASSP)*, May 2019.
- [47] Y. Yang, B. Zheng, S. Zhang, and R. Zhang, "Intelligent reflecting surface meets OFDM: Protocol design and rate maximization," *arXiv:1906.09956*, 2019.
- [48] T. L. Jensen and E. D. Carvalho, "On optimal channel estimation scheme for intelligent reflecting surfaces based on a minimum variance unbiased estimator," *arXiv:1909.09440*, 2019.
- [49] A. Alkhateeb, O. El Ayach, G. Leus, and R. W. Heath, Jr., "Channel estimation and hybrid precoding for millimeter wave cellular systems," *IEEE J. Sel. Topics Signal Process.*, vol. 8, no. 5, pp. 831-846, Oct. 2014.
- [50] M. E. Eltayeb, A. Alkhateeb, R. W. Heath, Jr., and T. Y. Al-Naffouri, "Opportunistic beam training with hybrid analog/digital codebooks for mmWave systems," in *Proc. IEEE Global Conf. Signal Inf. Process. (GlobalSIP)*, Orlando, FL, USA, Dec. 2015, pp. 315-319.
- [51] C. Liu, M. Li, S. V. Hanly, I. B. Collings and P. Whiting, "Millimeter wave beam alignment: Large deviations analysis and design insights," *IEEE J. Sel. Areas Commun.*, vol. 35, no. 7, pp. 1619-1631, Jul. 2017.
- [52] W. Tang, M. Z. Chen, X. Chen, J. Y. Dai, Y. Han, M. Di Renzo, Y. Zeng, S. Jin, Q. Cheng, and T. J. Cui, "Wireless communications with reconfigurable intelligent surface: Path loss modeling and experimental measurement," *arXiv:1911.05326*, 2019.
- [53] A. Alkhateeb, G. Leus, and R. W. Heath, Jr., "Compressed sensing based multi-user millimeter wave systems: How many measurements are needed?" in *Proc. IEEE Int. Conf. Acoust., Speech Signal Process. (ICASSP)*, Apr. 2015, pp. 2909-2913.
- [54] O. El Ayach, R. W. Heath, Jr., S. Abu-Surra, S. Rajagopal, and Z. Pi, "The capacity optimality of beam steering in large millimeter wave MIMO systems," in *Proc. IEEE SPAWC*, pp. 100-104, 2002.
- [55] S. Priebe, M. Kannicht, M. Jacob, and T. Kurner, "Ultra broadband indoor channel measurements and calibrated ray tracing propagation modeling at THz frequencies," *IEEE J. Commun. Netw.*, vol. 15, no. 6, pp. 547-558, Dec. 2013.
- [56] Q. H. Spencer, A. L. Swindlehurst, and M. Haardt, "Zero-forcing methods for downlink spatial multiplexing in multiuser MIMO channels," *IEEE Transactions on Signal Processing*, vol. 52, no. 2, pp. 461-471, Feb. 2004.
- [57] B. Ning *et al.*, "Channel Estimation and Transmission for Intelligent Reflecting Surface Assisted THz Communications," *arXiv:1911.04719*, 2019.